Sea surface chlorophyll signature in the tropical Pacific during eastern and central Pacific ENSO events

Marie-Hélène Radenac, Fabien Léger, Awnesh Singh, Thierry Delcroix

To cite this version:

Marie-Hélène Radenac, Fabien Léger, Awnesh Singh, Thierry Delcroix. Sea surface chlorophyll signature in the tropical Pacific during eastern and central Pacific ENSO events. Journal of Geophysical Research, 2012, 117 (C04007), 15 p. 10.1029/2011JC007841 . ird-00695543

HAL Id: ird-00695543
https://ird.hal.science/ird-00695543

Submitted on 9 May 2012

Sea surface chlorophyll signature in the tropical Pacific during Eastern and Central Pacific ENSO events

Marie-Hélène Radenac(*), Fabien Léger, Awnesh Singh, and Thierry Delcroix

LEGOS
UMR 5566 CNRS/IRD/CNES/UPS
14 avenue Edouard Belin
31400 Toulouse
France

(*) corresponding author: Marie-Hélène Radenac, IRD/LEGOS, UMR 5566, 14 avenue Edouard Belin, 31400 Toulouse, France (marie-helene.radenac@legos.obs-mip.fr)

Submitted to J. Geophys. Res. (2011JC007841). Revised version
7 February 2012

Abstract

Recent analyses of physical measurements show the existence of a Central Pacific type of El Niño (CPEN) with a sea surface temperature warming pattern distinct from that of the "classical" Eastern Pacific El Niño (EPEN). In this study, we analyze the surface chlorophyll signature of El Niño-Southern Oscillation (ENSO), using monthly maps of satellite-derived chlorophyll anomalies between September 1997 and December 2010. We identify five typical ENSO structures. The first structure describes the lonely 1997-1998 EPEN of the period, the second and third represent La Niña, the fourth illustrates intermediate conditions, and the fifth characterizes CPEN. During the 1997-1998 EPEN, a large eastward shift of the oligotrophic warm pool and a reduction of equatorial upwelling result in negative chlorophyll anomalies east of 170°E between 10°S and 10°N. During the four CPEN events, a reduced eastward shift yields negative chlorophyll anomalies in the equatorial band, within about 160°E and 160°W only. Westward surface current in the central basin limits the expansion of the anomaly core. Negative chlorophyll anomalies that extend eastward from the equatorial anomaly core probably result from reduced upward iron fluxes linked to the deepening of the Equatorial Undercurrent. During La Niña, the westward expansion of the equatorial upwelling results in positive chlorophyll anomalies west of the date line. Away from the equatorial band, advection of oligotrophic warm pool waters by enhanced eastward countercurrents drives negative anomalies within 8-10°N and towards the Marquesas Islands during CPEN, while reduced countercurrents leads to positive chlorophyll anomaly during La Niña.

1. Introduction

It is now well established that El Niño-Southern Oscillation (ENSO) events account for an important part of the global climate variability on interannual timescales with notable impacts on environment, ecosystems, economy, and society [Glantz, 2000; McPhaden et al., 2006]. Numerous studies have shown that sea surface temperatures (SST) warmer than seasonal values invade the central and, sometimes, the eastern equatorial Pacific during the warm phase (El Niño) of the ENSO cycle. However, many differences have been observed amongst the various El Niño events. Among those differences, warm SST anomalies occur both in the eastern and central Pacific during the conventional El Niño, also referred to as canonical, cold tongue, or eastern Pacific El Niño, whilst warm SST anomalies remain confined only in the central Pacific during most of the events observed in recent years [Trenberth and Stepaniak, 2001; Ashok et al., 2007; Kug et al., 2009; Kao and Yu, 2009]. Interestingly, this later type of events, referred to as central Pacific El Niño, dateline El Niño, or El Niño Modoki, has been shown to be more intense in recent decades [Lee and McPhaden, 2010] and could be more frequent in a warming world [Yeh et al., 2009]. Some studies argue that this later type of events differs from conventional ENSO [Ashok et al., 2007] while other studies argue that both types belong to an overall nonlinear phenomenon [Takahashi et al., 2011]. In this study, we will refer to these two types of El Niño as Eastern Pacific (EP) and Central Pacific (CP) El Niño.

Based on atmospheric observations, the well known Southern Oscillation Index (SOI) is often used to identify the warm and cold phases of ENSO. Based on oceanic observations, several SST indices were further proposed to distinguish the EP and CP El Niño. These mainly rely on comparisons between SST anomalies, normalized or not, in the Niño3 (5°S-5°N, 150°W-90°W) and Niño4 (5°S-5°N, 160°E-150°W) regions [Kug et al., 2009; Yeh et al., 2009; Kim et al., 2009]. Some studies also rely on other possible El Niño indices such as the Trans-Niño Index [TNI; Trenberth and Stepaniak, 2001], El Niño Modoki Index [EMI; Ashok et al., 2007], and other metrics [e.g. Kao and Yu, 2009; Takahashi et al., 2011; Ren and Jin, 2011]. Singh et al. [2011] also proposed ENSO indices based on differences of sea surface salinity (SSS) anomaly in two equatorial regions and in the South Pacific Convergence Zone (SPCZ). Identifications of EP and CP events following several of these methods are fairly consistent. Some discrepancies however exist and reflect the complexity of the problem as events may evolve from one type to the other [Yu and Kim, 2010; Takahashi et al., 2011] or may have patterns intermediate between the EP and CP types [Kug et al., 2009]. Table 1 summarizes the classification of EP and CP ENSO events since the strong El Niño in 1997-1998 (see also Table 1 in Singh et al. [2011] for previous years).

Although physical processes responsible for SST anomaly patterns during CP El Niño are, by far, not completely understood, they seem to differ from the ones leading to EP El Niño. Basically, during EP El Niño, the weakening of the trade winds and basin wide variations of thermocline depth lead to warming in the eastern equatorial Pacific while positive SST anomalies in the central basin result from eastward advection of the warm pool [Picaut et al., 2001; Vialard et al., 2001; Kao and Yu, 2009; Kug et al., 2009]. For CP El Niño, local atmospheric forcing and zonal advection are likely mechanisms involved in the development, confinement, and decay of anomalies in the central basin [Kao and Yu, 2009; Kug et al., 2009; Singh et al., 2011]. The so-called thermocline and advection feedbacks would then be at work during EP El Niño, while the advection feedback would mostly be at work during CP El Niño.

Mechanisms that control the SST warming during EP El Niño apparently account for the decrease of biological production in the equatorial Pacific. During the 1997-1998 El Niño, nutrient- and phytoplankton-poor (surface chlorophyll lower than 0.1 mg m^{-3}) waters of the warm pool were advected eastward to the central and eastern basins while vertical inputs of nutrients decreased in the east because of the thermocline deepening and the reduction of the upward vertical velocity [Chavez et al., 1998; Radenac et al., 2001]. The ecosystem of the equatorial upwelling region is iron-limited [Landry et al., 1997] and the thermocline deepening is associated with the depression of the Equatorial Undercurrent (EUC) that transports iron across the basin from the western Pacific [Gordon et al., 1997; Wells et al., 1999; Lacan and Jeandel, 2001]. As biologically available iron in the photic layer is mainly upwelled from the EUC [Gordon et al., 1997], strong reduction of the iron fluxes ensues from the depression of the EUC during El Niño [Barber et al., 1996; Gordon et al., 1997; Chavez et al., 1999; Friedrichs and Hofmann, 2001]. The result is a collapse of new and primary production in the equatorial Pacific during the 1997-1998 [Chavez et al., 1999; Strutton and Chavez, 2000; Radenac et al., 2001; Turk et al., 2001] and previous EP El Niño events [Barber and Kogelschatz, 1990; Barber et al., 1996]. However, to our knowledge, no study characterizes the response of the equatorial ecosystems to the subsequent CP El Niño events in 2002-2003, 2004-2005, 2006-2007, and 2009-2010, apart from the recent paper by Turk et al. [2011]. This is the goal of this study. The occurrence and strength of CP El Niño have increased since the 1990s (Lee and McPhaden, 2010) and their frequency may still increase in future as stressed by Yeh et al. (2009). Therefore, further investigations are necessary to better understand ENSO related physical-biological interactions and their impacts on biological fields and dynamics up to top predators.

The manuscript is organized as follows. Section 2 describes the satellite-derived data that allow us to describe the 1997-2010 changes in surface chlorophyll on basin scale. To set the context, section 3 compares the SST, SSS, and surface chlorophyll anomalies in the equatorial band. Then, section 4 contrasts the surface chlorophyll anomaly signatures characterizing the EP and CP El Niño, and section 5 analyzes the possible impacts of changes in surface circulation and thermocline depth on the surface chlorophyll distribution. A discussion and conclusion appear in the last section.

2. Data and methods

Surface chlorophyll concentrations were derived from Sea-viewing Wide Field-of-view Sensor (SeaWiFS) measurements and from the Moderate Resolution Imaging Spectroradiometer (MODIS) measurements aboard the Aqua satellite. SeaWiFS data are available between September 1997 and December 2010 and MODIS data since July 2002. We used 9 km resolution monthly composites computed by the NASA Goddard Space Flight Center (GSFC) Distributed Active Archive Center (DAAC) [McClain et al., 2004]. When a SeaWiFS monthly map was not available or had less than 60% of data available (7 maps, i.e. 4.4% of the time), we used the Aqua MODIS map in order to obtain a complete chlorophyll time series from September 1997 to December 2010. For each location, chlorophyll values higher than 3 mg m^{-3} and/or that were more than five standard deviations away from the 1997-2010 mean were treated as missing (Messié and Radenac, 2006). In the calculations, we interpolated the data onto a 1°×1° grid following the method of Yoder and Kennelly [2003]. First, we computed 0.25°×0.25° maps using the maximum likelihood estimator [Campell et al., 1995]. Then, most of the data gaps due to sparse clouds were filled by taking the median of every 1°×1° cell. The remaining missing data were filled by taking the median of the first neighbors. The chlorophyll anomalies we present are relative to a mean seasonal cycle calculated between 1998 and 2010. We also used monthly maps of Photosynthetically Available Radiation (PAR) estimates derived from SeaWiFS and MODIS [Frouin et al., 2003].

SST data was provided by the Hadley Centre for Climate Prediction and Research Sea Ice and Sea Surface Temperature HadISST1 dataset [Rayner et al., 2003]. Monthly SST maps are available since 1870 on a 1°×1° grid. SSS data came from the recently-updated Delcroix et al. [2011] product for the tropical Pacific. Monthly SSS data are available on a 1°×1° grid and span from 1950 to 2009. Monthly near surface currents were obtained from the Ocean Surface Current Analysis - Real time (OSCAR) 1°×1° product; the geostrophic, wind-driven, and thermal-wind components of which are derived from satellite data [Bonjean and Lagerloef, 2002]. Monthly anomalies of wind speed and depth of the 20°C ($Z_{20°C}$) isotherms are derived from time series recorded at the Tropical Atmosphere Ocean/Triangle Trans Ocean Buoy Network [TAO/TRITON; McPhaden et al., 1998] moorings. We also used time series of the SOI and EMI [Ashok et al., 2007].

Different statistical procedures have been used in the literature to discriminate ENSO features. To name a few, these include regression of anomaly onto specific ENSO indices [Trenberth and Stepaniak, 2001; Ren and Jin, 2011; Takahashi et al., 2011; Singh and Delcroix, 2011], Empirical Orthogonal Functions (EOF) analyses [Ashok et al., 2007; Park et al., 2011], combined regression-EOF analyses [Kao and Yu, 2009], neural network [Hsieh, 2001; Leloup et al., 2007], and Agglomerative Hierarchical Clustering (AHC) analysis [Kao and Yu, 2009; Singh et al., 2011]. We tested here the EOF and AHC analyses on chlorophyll in the tropical Pacific. The EOF analysis of the chlorophyll anomaly indicates that the CP El Niño signal is distributed over at least the first, third, and fourth modes (not shown). Hence, the EOF technique does not distinguish properly EP and CP El Niño. A similar leakage of the signal was found for the EOF analysis of SSS in the tropical Pacific [Singh et al., 2011]. Therefore, we chose to perform an AHC analysis on the monthly surface chlorophyll anomalies to characterize ENSO related signatures. In this nonlinear composite procedure, maps are merged into clusters according to their similarity, estimated from the smallest Euclidean distance (defined as the root-mean-squared distance between each pairs of maps). The clustering procedure can be represented by a dendrogram tree that illustrates combinations made at each successive step of the analysis. This technique has been successfully performed on SST [Kao and Yu, 2009], SSS [Singh et al., 2011], and South Pacific Convergence Zone (SPCZ) location [Vincent et al., 2009] to separate ENSO signatures in the tropical Pacific. In this study, we applied the AHC method to monthly maps of surface chlorophyll anomalies for the region between 130°E-70°W and 10°S-10°N. The Indonesian Throughflow region and Central and South America coastal upwellings were excluded as regional effects may mask the basin-scale ENSO signature (Fig. 1).

3. Comparing SST, SSS, and surface chlorophyll anomalies in the equatorial band

The mean chlorophyll distribution and its interannual variability are presented first to set the context (Fig. 1). The mean values were computed by averaging all monthly values covering the 1997-2010 period, and the interannual variability was defined as the standard deviation of the chlorophyll anomalies (relative to the mean seasonal cycle). Figure 1a shows that the mean chlorophyll is lower than 0.3 mg m^{-3} outside the Central and South America upwelling regions, with well-marked maxima in a huge equatorial region spreading westward from the South American coast. These values are mostly due to the equatorial upwelling which brings cool, salty, and nutrient-rich waters toward the surface. Although the surface nitrate concentration is high in the upwelling, the chlorophyll content remains moderate (less than

0.2 mg m^{-3} on average) because of an iron-limited and grazing-balanced ecosystem [Landry et al., 1997]. Mesotrophic waters of the equatorial upwelling are surrounded by oligotrophic waters ([chl] < 0.1 mg m^{-3}) of the warm pool to the west and of subtropical gyres poleward (note also the moderate mesotrophic waters north of Papua New Guinea and near the Solomon Sea). The interannual variability (Fig. 1b) is high between 10°S and 10°N, especially along the equator, in the North Equatorial Countercurrent (NECC) region, around Papua New Guinea, and in the Central and South America coastal upwelling regions.

Looking at the regions of maximum interannual variability, the longitude-time distributions of the 5°N-5°S averaged SST, SSS, and surface chlorophyll anomalies are shown in figure 2. For all El Niño events, the maximum positive SST anomaly occurs during boreal winter, between September and February (Fig. 2a). The location and amplitude of the anomaly differ from one event to the other. The 1997-1998 (EP, see Table 1 and below) El Niño is the only one with very warm SST anomaly (SSTA > 3°C) that peaks east of 120°W and extends toward the central basin. During the following (CP, see Table 1 and below) El Niño events, the maximum SST anomaly is lower (sometimes less than 1°C) and mostly situated in the central-western basin, at least in 2002-2003, 2004-2005, and 2009-2010. The strongest warming (SST anomaly close to 2° C) during a CP El Niño event is reached during the mature phase of the 2009-2010 event, in agreement with Lee and McPhaden [2010].

The strongest negative SSS anomalies (Fig. 2b) appear to be located west of the maximum positive SST anomalies. During the 1997-1998 EP El Niño, the SSS anomaly is negative east of 160°E, with a maximum freshening near the date line. During the following CP El Niño events, the maximum negative anomalies tend to be displaced westward by 10 to 15° of longitude, except in 2002-2003, in agreement with Singh et al (2011).

The time series of surface chlorophyll anomaly (Fig. 2c) is reminiscent of the SSS anomaly time series as strong negative chlorophyll anomalies tend to be located west of the warm El Niño-related SST anomalies. In 1997-1998, the strong anomaly core (< -0.12 mg m^{-3}) is near 150°W and the surface chlorophyll concentration is below the mean seasonal value from 150°E to the American coast. During the following events, the negative anomaly core (-0.08 to -0.10 mg m^{-3}) is located in the central-western basin, between about 150°E and 180°, while the moderate anomalies observed eastward range between less than -0.02 mg m^{-3} in 2002-2003 and 2004-2005 to -0.04 mg m^{-3} in 2006-2007 and 2009-2010.

Oligotrophic waters ([chl] < 0.1 mg m^{-3}) have been shown to be quasi-persistent in the eastern part of the equatorial warm pool while moderate mesotrophic waters (surface chlorophyll concentration slightly higher than 0.1 mg m^{-3}) were often observed in its western part [Radenac et al., 2010]. This oligotophic region is delimited by the black contour in Figures 2a, b, c. The easternmost limit of this zone characterizes the eastern edge of the warm pool [Murtugudde et al., 1999; Stoens et al., 1999; Radenac et al., 2010] that separates waters of the eastern warm pool ([chl] < 0.1 mg m^{-3}) from upwelled waters ([chl] > 0.1 mg m^{-3}). Large zonal displacements of the eastern edge of the warm pool occur at interannual timescales and its longitudinal position is related to the phases of ENSO [Picaut and Delcroix, 1995; Le Borgne et al., 2002]. It reaches 130°W during the 1997-1998 EP El Niño and lies between the dateline and 160°W during CP events. Interestingly, the oligotrophic waters of the eastern part of the warm pool follow these movements (Fig. 2c). Thus, the maximum negative chlorophyll and SSS anomaly cores are both located west of the warmest SST anomalies.

Several La Niña years interleave between El Niño years (Table 1). When La Niña events reach their mature phase in boreal winter (e.g. in early 2008), SST in the central and eastern basins are cooler while becoming slightly warmer west of 160°E (Fig. 2a). Strong positive anomalies of SSS and surface chlorophyll are closely related west of 150°W (Figs. 2b, c). They are located at the western limit of the cool SST anomaly, in the region of zonal displacements of the eastern edge of the warm pool. Chlorophyll anomalies exceed 0.10 mg m^{-3} in 2010 and range between 0.05 and 0.08 mg m^{-3} during the other La Niña years. A moderate increase of chlorophyll (< 0.03 mg m^{-3}) is observed eastward of these maxima.

Figure 2c shows that the chlorophyll anomalies are negative all along the equator in 1997-1998 while the core of chlorophyll anomaly remains west of 150°W during the following boreal winters (see also spatial patterns from the cluster analysis below). Therefore, comparing the chlorophyll anomalies averaged over the Niño3 and Niño4 regions during the peak period of the events (September-February; Fig. 3) mostly concurs with the classification of La Niña and CP and EP El Niño events. Chlorophyll anomalies are negative in both regions during El Niño years (SOI < 0) and positive during La Niña years (SOI > 0). Also, differences between the anomalies in each region are consistent with the CP El Niño as depicted by the EMI (Fig. 3). The amplitude of the chlorophyll anomaly indeed tends to be greater in Niño4 than in Niño3 during CP El Niño (EMI > 0). Following these results, the 2006-2007 El Niño is identified here as a CP event as in the SSS study [Singh et al., 2011] and in contrast to most of the SST studies (Table 1). The 2009-2010 event, acknowledged as the warmest CP El Niño during the last decades [Lee and McPhaden, 2010], yields chlorophyll anomalies in Niño4 weaker than during the 2002-2003 event. Actually, the magnitude of the chlorophyll decrease in Niño4 is linked to the eastward expansion of the oligotrophic warm pool (Fig. 2c) whereas warming in Niño4 is not (Fig. 2a). During La Niña winters, the chlorophyll anomaly in Niño4 is always larger than in Niño3 (except in 1998-1999), suggesting that the strongest increase of chlorophyll occur in the region of zonal shifts of the eastern edge of the warm pool. The greatest winter increase reached in the Niño4 region is in 2010-2011.

4. Describing the spatial patterns of ENSO-related surface chlorophyll anomalies

Using the AHC analysis described in section 2, we identified five clusters out of 160 monthly maps during the September 1997-December 2010 period. As detailed below, we believe they are representative of EP El Niño, equatorial recovery, La Niña, intermediate CP El Niño, and CP El Niño conditions. They occur about 6%, 6%, 34%, 28%, and 26% of the time, respectively. The associated time series and the derived composite maps are presented in figure 4. Occurrences of EP El Niño (1997-1998), CP El Niño (2002-2003, 2004-2005, 2006-2007, 2009-2010), and La Niña events (1998-1999, 1999-2000, 2000-2001, 2007-2008, 2008-2009, 2010-2011) are consistent with those found in previous studies using SST or SSS indices (Table 1) and with the comparison of chlorophyll anomalies in the Niño3 and Niño4 regions (Fig. 3). Of note, the cluster analysis does not classify the end of 1998 as typical La Nina conditions although that period has been described as a La Niña year from the surface chlorophyll distribution [Murtugudde et al., 1999; Radenac et al., 2001; Ryan et al., 2002] and from other variables (Fig. 3; Table 1): the reason for this is discussed below. Intermediate CP El Niño periods occur in 2001-2002, 2003-2004, 2005-2006, and 2007 near CP El Niño years when the SOI or EMI is weak (Fig. 3).

Aside from the “all-month” AHC analysis we present, we also performed an AHC analysis using September to February months only (not shown) because CP and EP El Niño and La Niña events reach their mature phase in boreal winter for most climate variables [Kao and Yu, 2009] and for chlorophyll changes [Chavez et al., 1999; Strutton and Chavez, 2000; Radenac et al., 2001; see also Figure 2]. In that case, we obtained similar patterns for the CP and EP El Niño, and La Niña clusters. The strong equatorial signal (Fig. 4c) however did not show up as elevated chlorophyll concentration along the equator was observed in boreal spring and summer. Caution is thus required when selecting some months per year only in analyzing ENSO features.

Cluster 1 captures the spatial pattern of the only EP El Niño event over the study period (Fig. 4b). Given the strength of this event, it is not surprising that its spatial pattern resembles that of the EOF analysis performed on the 1997-1999 chlorophyll data [Wilson and Adamec, 2001]. The chlorophyll anomaly is negative over a broad region from 170°E to the American coast and maximum along the equator. The northern limit of the negative anomaly region is sharp and almost zonally oriented near 8°N while the southern limit may look smoother and extends south of 10°S (except west of the dateline). Unlike the SST anomaly pattern during EP El Niño, which is strongest near the American coast and extends westward along the equator [Rasmusson and Carpenter, 1982; Kao and Yu, 2009; Kug et al., 2009], the chlorophyll anomaly seems to have two distinct cores (lower than -0.075 mg m^{-3}). One core is found between the date line and 140°W and the other one east of 110°W in the equatorial region. The chlorophyll anomaly is positive in the western basin mostly between the equator and 10°latitudes.

Characteristics of surface chlorophyll during the four CP El Niño events are represented by cluster 5 (Fig. 4f). The negative anomaly pattern has an arrow shape whose head would be the core of the largest negative anomaly (less than -0.08 mg m^{-3}) located at the equator around 170°E. Thin bands of negative chlorophyll anomaly (-0.02 to -0.01 mg m^{-3}) stretches from the anomaly core along 8-10°N to the Central American coast, while another of lower magnitude extends to the Marquesas Islands at 140°W, 10°S. The tail of the arrow would be the narrow band of moderate negative anomaly (-0.03 to -0.02 mg m^{-3}) along the equator from the anomaly core to the American coast. The core of maximum negative surface chlorophyll anomaly matches the core of maximum negative SSS anomaly [Singh et al., 2011] during both El Niño types, and in the same way as the SST anomaly, it is shifted westwards during CP El Niño compared to EP El Niño. The three zonal bands of moderate negative chlorophyll anomaly that stretch eastward from the equatorial minimum anomaly core are specific to the chlorophyll signature. In the western Pacific, north of Papua New Guinea and Solomon Islands, chlorophyll anomalies are positive during CP El Niño events.

The timing of La Niña years, captured by cluster 3 (Fig. 4a), are consistent with the occurrence of positive SOI (Fig. 3). The La Nina patterns (Fig. 4d) somewhat mirror the CP El Nino patterns (Fig. 4f) in the western half of the basin, although the maximum anomaly is stronger and extends 5° to 10° longitude further to the west during La Niña. In agreement with figure 3, cluster 3 thus shows that the positive chlorophyll anomalies in Niño4 region are larger than in Niño3 (Fig. 4d). Narrow bands of positive anomaly stretch from the high positive anomaly core along the equator and 6°N -7°N toward the American coast and to the Marquesas Islands. Cluster 2 captures a strong enhancement of the surface chlorophyll concentration (> 0.05 mg m^{-3}) in a narrow equatorial band by the end of 1998 and mid-2010 (Fig. 4a, c) during the strong La Nina events that followed the strong 1997-1998 EP El Niño and 2009-2010 CP El Niño. Two cores with chlorophyll anomaly higher than 0.08 mg m^{-3} are located west of the Kiribati Islands (175°E) and between 140°W and 120°W. Anomalies are negative between 10°S and 10°N in the western basin and poleward of 5° in the east.

Surface chlorophyll distribution captured by cluster 4 (Fig. 4a, e) appears when the SOI and chlorophyll anomalies in the Niño3 and Niño4 regions are weak (Fig. 2). The main feature is a negative anomaly zone in the western equatorial basin.

5. Analyzing possible drivers of surface chlorophyll changes during El Niño events

In this section, we investigate mechanisms that could possibly constrain the overall spatial structure of surface chlorophyll anomaly during El Niño events, relying on changes in surface zonal current, wind, and thermocline depth (assumed to be the 20°C isotherm depth, $Z_{20°C}$). We first recall the main results obtained for the 1997-1998 EP El Niño [Chavez et al., 1999; Murtugudde et al., 1999; Stoens et al., 1999; Wilson and Adamec, 2001; Strutton and Chavez, 2000; Radenac et al., 2001; 2005]. Then, we choose to describe the spatial evolution of chlorophyll anomaly during CP El Niño, with a slight focus on the fairly representative 2002-2003 event, rather than on a composite, in order to preserve tiny structures whose positions are slightly different among events. Figure 5 shows the time evolution of the anomalies of zonal wind speed, $Z_{20°C}$, and surface zonal current along the equator from September 1997 to December 2010. The limits of the oligotophic region are indicated by the black contour in each panel. Anomalies of the surface current are superimposed on the surface chlorophyll anomalies during the peak period (September-February) of the 1997-1998 EP El Niño (Fig. 6) and 2002-2003 CP El Niño (Fig. 7).

5.1. The 1997-1998 EP El Niño event

During boreal fall of 1997, strong anomalous eastward currents dominate the equatorial Pacific (Fig. 5c; Fig. 6a-d) as a consequence of anomalous westerly winds (Fig. 5a) and forced downwelling Kelvin waves [Delcroix et al., 2000]. The South Equatorial Current (SEC) is weak or reversed and the NECC is stronger and shifted southwards [Johnson et al., 2000]. As a result, nutrient-poor warm pool waters are advected eastward and reach 130°W during the mature phase in November 1997-January 1998 [Radenac et al., 2001]. The core of high negative chlorophyll anomaly is in the eastern part of the warm pool (Fig. 2c, 4b) where eastward surface currents are strong (Fig. 5c). Meanwhile, vertical supplies of nitrate and iron decrease or cease because of the reduction of the upwelling and the deepening of the nitracline and EUC [Fig. 5b; Chavez et al., 1999; Strutton and Chavez, 2000; Wilson and Adamec, 2001; Radenac et al., 2001; 2005]. A combination of these processes lead to a dramatic decrease of the surface chlorophyll and of the biological production in the central and eastern basins. The northern and southern limits of the negative chlorophyll anomaly closely match the extent of the eastward surface current anomaly until the peak period in December 1997 (Fig. 6a-d). Starting in January 1998, the surface chlorophyll anomaly weakens as strong westward surface currents begin to develop (Fig. 6d-e).

In the warm pool, the overall chlorophyll increase (Fig. 6a-f) has been ascribed to the thermocline rise (Fig. 5b) allowing nutrient input toward the lighted layer [Wilson and Adamec, 2001; Radenac et al., 2001; Turk et al., 2001]. Part of it, between 5°N and 10°N, results from enhanced chlorophyll concentration in the meanders of the nascent NECC observed seasonally between January and June and that were strong at the end of the 1997-1998 El Niño [Christian et al., 2004; Messié and Radenac, 2006]. Upwelling that develops along the coast of Papua New Guinea and Solomon Islands during favorable periods of westerly wind [Webster and Lukas, 1992; Kuroda, 2000; Ueki et al., 2003] also contributes to the chlorophyll increase in the warm pool south of the equator [Messié, 2006; Radenac et al., 2010].

5.2. The CP El Niño events

During CP El Niño events, the eastward shift of the warm pool (see the black contours in figure 5a) in response to westerly winds is of lesser magnitude than during EP El Niño. The associated equatorial eastward surface currents contribute to the development of negative chlorophyll anomaly as a consequence of the penetration of the oligotrophic waters of the warm pool toward the mesotrophic waters of the upwelling (Fig. 5c). The core of high chlorophyll anomaly remains within the zone of quasi-persistent oligotrophic waters enclosed by the 0.1 mg m^{-3} surface chlorophyll isoline in the eastern part of the warm pool (Fig. 2c), near the zone of convergence between the eastward surface current in the warm pool and the westward SEC east of it (Fig. 5c). The importance of this current convergence has been raised by Kug et al. [2009] and Singh et al. [2011] to explain how SST and SSS anomaly cores could remain confined in the central basin during CP El Niño.

During the 2002-2003 CP El Niño, the maximum negative chlorophyll anomaly is situated around 170°E in June, 180°E in August, and it stays at 170°W between September and December 2002 (Fig. 2c, 7a-d). It starts to move back to the west in January 2003 when strong westward anomalies develop. The monthly maps of surface chlorophyll and current (Fig. 7a-c) also suggest that anomalous eastward currents partly contribute to the equatorial chlorophyll decrease towards the American coast.

As discussed above for CP El Nino, negative anomalies (weaker than -0.015 mg m^{-3}) are constrained within 2° of the equator east of the high chlorophyll anomaly core (Fig. 4f). The zonal wind anomaly is slightly westward in the eastern basin during the CP El Niño years (Fig. 5a) and so cannot be responsible for a collapse of the upwelling in this region. Besides, variations of the vertical supply of nitrate, depending on the nutrient pool depth represented by the 20°C isotherm depth ($Z_{20°C}$), will not impact the phytoplankton growth as nitrate is usually in excess in this region. The equatorial chlorophyll decrease would rather be the result of vertical displacements of the EUC that contribute modulating vertical iron fluxes and the phytoplankton growth in the iron limited ecosystem of the central and eastern equatorial Pacific. The temporal variability of the $Z_{20°C}$ anomaly can be used as an indicator of the EUC depth (Z_{EUC}) anomaly (Izumo, 2005). When ADCP currents are available at the equatorial mooring sites, the bias between Z_{EUC} (calculated as the depth of the maximum eastward velocity) and $Z_{20°C}$ is lower than 4 m at 170°W and 140°W and the correlation coefficient is 0.72 at both sites. Therefore, the variations of $Z_{20°C}$ reliably represent the variations of Z_{EUC} that deepens by 20-40 m during CP El Niño (Fig. 5b) and could drive a significant decrease of the vertical iron flux [Chavez et al., 1999]. A strip of maximum anomaly confined to the equator is consistent with the structure of meridional velocity and a narrow band of strong divergence roughly centered along the equator [Poulain, 1993]. This further suggests that biology along the equator is sensitive to the EUC depth and iron concentration.

Off the equator, the narrow zonal band of negative chlorophyll anomaly between 5°N and 10°N is observed during the four CP El Niño events. During the 2002-2003 CP El Niño event, it appears during August-September (Fig. 7a) and starts to break up during January-February (Fig. 7e). The negative chlorophyll anomaly strip follows the position of the eastward surface current anomaly (Fig. 7a-d), suggesting that nutrient- and phytoplankton-poor water from the warm pool is advected eastward by the strong NECC. Messié and Radenac [2006] showed the significant impact of the NECC variations on the surface chlorophyll seasonal variability in the western Pacific. During El Niño events, it is a basin-wide feature that participates in setting up the sharp chlorophyll front at the northern edge of the upwelling. In monthly chlorophyll maps, it is seen as a narrow band of oligotrohic waters extending from the warm pool to the Central American coast during October-December of all El Niño years (not shown). South of the equator, negative chlorophyll anomalies coincide with a region of southeastward surface currents that transport nutrient- and phytoplankton-poor waters toward the Marquesas Islands (Fig. 7a-f). This feature is observed during September-February 2002-2003, 2004-2005, and 2006-2007. It develops later during February-April during the 2009-2010 CP El Niño event (not shown).

6. Summary and discussion

Enhanced attention has been given to global climate changes related to differences in the location of SST anomalous warming in the tropical Pacific in recent years [Trenberth and Stepaniak, 2001; Ashok et al., 2007; Kug et al., 2009; Kao and Yu, 2009; Yeh et al., 2009; Lee and McPhaden, 2010]. To our knowledge, no attempt has been made so far to contrast the biological conditions featuring the EP and CP El Niño, except for the recent study by Turk et al. [2011]. To fulfill this gap, the goal of our study was to contrast and tentatively explain the signature in chlorophyll of the EP and CP ENSO, for the 1997-2010 period.

During the SeaWiFS years, an AHC analysis of the surface chlorophyll anomaly shows that EP El Niño occurred in 1997-1998, CP El Niño in 2002-2003, 2004-2005, 2006-2007, and 2009-2010, while La Niña lasted from 1998 to 2001 and from 2007 to 2009, consistent with previous studies based on SST and SSS analyses (Table 1). Both types of El Niño events are associated with an overall decrease of surface chlorophyll in the 10°S-10°N region. Yet, spatial patterns differ between events.

During the 1997-1998 EP El Niño event, negative anomalies occupy most of the equatorial basin between 10°S and 10°N, except for a chlorophyll increase in the western basin. A strong negative chlorophyll anomaly (< -0.075 mg m^{-3}) is located at the equator between the date line and 150°W and the oligotrophic warm pool is displaced eastward and reaches 130°W.

During the CP El Niño events, the equatorial anomaly is weaker (< -0.045 mg m^{-3}), shifted westwards by about 20° of longitude, and the eastern edge of the oligotrophic warm pool is confined west of 160°W. So, as already found for SST and SSS [Kug et al., 2009; Singh et al., 2011], the region of strong chlorophyll anomaly is clearly shifted westward during CP El Niño relative to EP El Niño. The location of these strong negative anomalies in the eastern part of the warm pool suggests that oligotrophic waters of the warm pool replace mesotrophic waters of the upwelling in the central basin, and that zonal advection is a major process responsible for this signature. During CP El Niño, westward surface currents in the eastern and central basins probably limit the eastward spreading of the negative chlorophyll anomaly core.

Other mechanisms affecting nutrient or light availability could also lead to a chlorophyll decrease in the central equatorial basin. One of them is the depth of the nutrient pool. The core of high chlorophyll anomaly matches the maximum sea level anomaly [Kug et al., 2009; Bosc et al., 2009] which reflects a strong depression of the thermocline [Rébert et al., 1985], closely related to the depth of the nitracline in the oligotrophic warm pool. Besides, barrier layer tends to be thick in the eastern edge of the warm pool [Maes et al., 2004; Bosc et al., 2009] and to further isolate the deep nutrient pool from the lighted surface layer [Mackey et al., 1995; Eldin et al., 1997; Murtugudde et al., 1999; Turk et al., 2001]. The nutrient pool is deep on average in the oligotrophic warm pool and the depression of the nitracline in the eastern part of the warm pool is probably a second order factor on surface chlorophyll changes compared to the impact of advection.

Another factor accounting for chlorophyll changes during EP and CP El Niño could be the reduction of incident light in the central Pacific as suggested by Park et al. [2011]. Zonal extension of oligotrophic conditions is linked to the zonal extension of the warm pool, which is the site of convective activity and moves eastward during El Niño. The average monthly value of the satellite derived Photosynthetically Available Radiation (PAR) is 44.7 ± 4.4 Einstein m^{-2} d^{-1} in the eastern part of the warm pool while it is 48.6 ±2.2 Einstein m^{-2} d^{-1} in the upwelling region at 140°W. The eastward shift of the convection zone leads to PAR anomaly around 10 Einstein m^{-2} d^{-1} in the strong chlorophyll anomaly region in 1997-1998 and close to or less than 5 Einstein m^{-2} d^{-1} during the following El Niño events. These relatively weak PAR variations, three to ten times weaker than variations at mid and high latitudes [Letelier et al., 2004; Goes et al., 2004], suggest a weak impact on the phytoplankton growth. Therefore, zonal advection and the resulting change of ecosystem in the central Pacific are probably the dominant mechanisms responsible for the strong chlorophyll anomaly, as also proposed by Messié and Chavez [submitted to J. Geophys. Res., 2012]. Mesotrophic waters of the upwelling with surface chlorophyll concentration around 0.2 mg m^{-3} are replaced by oligotrophic waters of the eastern part of the warm pool with surface chlorophyll concentration lower than 0.07 mg m^{-3} [Radenac et al., 2010]. However, separating the impact of the ecosystem change and of the light attenuation is not simple as oligotrophic waters move simultaneously to the convection zone, and a process study is needed to estimate each influence.

We suggest that the chlorophyll decrease along the equator east of the strong central Pacific anomaly is the consequence of reduced vertical iron fluxes linked to the deepening of the EUC during El Niño [Barber et al., 1996; Chavez et al., 1999; Wilson and Adamec, 2001;

Friedrichs and Hofmann, 2001]. Changes in the iron content of the EUC could also impact biology in the central and eastern Pacific. Ryan et al. [2006] hypothesized that the strengthening of the New Guinea Coastal Undercurrent (NGCUC), flowing northwestward along the northern coast of Papua New Guinea, favored transport of iron from shelf sediments that feeds the EUC during El Niño years, which in turn favored phytoplankton blooms observed in the central Pacific following El Niño events. In contrast, setting the iron concentration proportional to the NGCUC speed in the source region did not change the intensity of eastern equatorial Pacific blooms in a simulation based study [Gorgues et al., 2010]. Thus, although the impact of a continental iron source in the western equatorial Pacific on the biogeochemistry of the equatorial upwelling region has been shown in several modeling studies [Christian et al., 2002; Vichi et al., 2008; Slemons et al., 2009; Gorgues et al., 2010], the influence of a variable iron supply into the EUC on the ecosystems of the central and eastern basins is still unclear. So is the role of tropical instability waves (TIW). Because of vigorous horizontal processes as well as upwelling and downwelling, localized maximum and minimum of phytoplankton biomass characterize TIW [Yoder et al., 1994; Strutton et al., 2001; Menkes et al., 2002]. Their net impact on phytoplankton biomass has been estimated to be positive [Barber et al., 1996; Friedrichs and Hofmann, 2001; Strutton et al., 2001] or negative [Gorgues et al., 2005]. Other studies show an enhancement or decrease of the phytoplankton biomass depending on interactions between the large scale thermocline/ferricline depth and the intensity of the local TIW dynamics [Vichi et al., 2008; Evans et al., 2009]. The reduction or absence of TIW activity during El Niño [Legeckis, 1977; Friedrichs and Hofmann, 2001; Evans et al., 2009] can also possibly contribute to the chlorophyll decrease observed along the equator.

The AHC analysis of the 1997-2010 surface chlorophyll anomaly dataset does not separate La Niña events into EP and CP events. Chlorophyll increases in the equatorial western basin and near 8-10°N and toward the Marquesas Islands are common patterns to La Niña maps. Nevertheless, the location of the equatorial core of positive anomalies and its magnitude change (much stronger in 2010 than during other events) and an equatorial increase in the central and eastern basins may not be observed. The average location of chlorophyll anomaly of the six La Niña events seen by SeaWiFS is situated west of the EP and CP El Niño anomalies. This is consistent with the La Niña signature as reported by Kug et al. [2009] and Kug and Ham [2011] who do not separate CP and EP cold events in terms of SST anomaly. Besides, the chlorophyll anomaly analysis does not evidence any symmetry between the warm and cold phases of ENSO events as suggested in Kao and Yu [2009] and Yu et al. [2010] analyses. The distinct EP and CP La Niña patterns mentioned by Singh et al. [2011] are based on a cluster analysis of SSS that captures a signal in the SPCZ region that does not show up in the chlorophyll analysis.

During La Niña years, the equatorial core of positive anomaly results from the westward expansion of the upwelling mesotrophic waters in a region where the usual surface chlorophyll concentration does not exceed 0.1 mg m^{-3} (Fig. 2c). The weak nutrient supply to the euphotic layer in the Niño4 region results from horizontal advection of nutrient-rich waters from the east and upward advection [Stoens et al., 1999]. During La Niña events, observational and modeling studies have shown that upwelling led to increased surface chlorophyll concentration in the western Pacific [Blanchot et al., 1992; Radenac and Rodier, 1996; Radenac et al., 2001]. East of the strong anomaly core, the iron limitation and the grazing pressure (small phytoplankton and zooplankton species dominate the ecosystem and microzooplankton can quickly respond to changes in nano- and pico-phytoplankton biomass) control the ecosystem resulting in a monotonously low phytoplankton biomass in the equatorial divergence [Chavez et al., 1991; Le Bouteiller and Blanchot, 1991; Strutton et al., 2008]. This special feature of the equatorial upwelling ecosystem could explain why no strong chlorophyll increase characterizes the overall La Niña distribution of chlorophyll anomaly along the equator east of the anomaly core (Fig. 4d). An asymmetry between El Niño and La Niña has also been observed in terms of temperature (Larkin and Harrison, 2002; An and Jin, 2004). The warm phase of ENSO is often stronger than its cold phase. Nonlinear dynamical processes could impact nutrient (iron) supply and cause an asymmetry of the ENSO-related biological response as they impact the ENSO-related heat budget (An and Jin, 2004). More investigations remain to be done on this issue, especially during the CP El Niño events that dominate during the recent years. Cluster 2 in the AHC analysis (Fig. 4a, c) captured exceptions to this uniformity. 80% of the maps that compose this cluster come from the 1998 La Niña year when unusual large-scale blooms [Ryan et al., 2002] were observed in the equatorial Pacific after the major 1997-1998 EP El Niño event. Chlorophyll increases subsequent to island mass effect generated by the Kiribati Islands, which behave as an obstacle to both the SEC and the EUC between February and June 1998 [Ryan et al., 2002; Messié et al., 2006] may contribute to the positive anomaly observed west of the dateline. A second bloom, the longest and more intense one with chlorophyll concentration higher than 0.8 mg m^{-3}, developed between 160°W and 140°W and then spread eastward from June to September [Chavez et al., 1999; Ryan et al., 2002; Gorgues et al., 2010]. The last bloom was observed around 130°W during November-December 1998 [Ryan et al., 2002]. Reasons for these blooms can be both large-scale and local dynamics, such as, enhanced iron vertical fluxes because of a shallower thermocline and more active TIW during La Niña. A similar but somewhat weaker situation seemed to occur in mid-2010. Interestingly, these equatorial recovery conditions occur when strong El Niño events turn swiftly into strong La Niña: from the major 1997-1998 EP El Niño to the strong 1998-1999 La Niña [Chavez et al., 1999; Ryan et al., 2002; Radenac et al., 2010] and from the strong 2009-2010 CP El Niño to the strong 2010-2011 La Niña [Kim et al., 2011]. These periods coincide with phases of reduced grazing pressure as a response to El Niño related reduced phytoplankton biomass and productivity. Therefore, momentarily low grazing pressure probably combines to dynamical impacts leading to enhanced phytoplankton growth to drive high phytoplankton biomass during these recovery periods after strong El Niño events [Strutton and Chavez, 2000; Friedrichs and Hofmann, 2001; Gorgues et al., 2010].

While increased eastward advection was responsible for the chlorophyll decreases along 8-10°N and towards the Marquesas Islands during CP El Niño, the chlorophyll increases at the same locations during La Niña coincide with increased westward and poleward surface currents suggesting the influence of horizontal advection.

Situations that occurred in 2001-2002, 2003-2004, 2005-2006, and 2007 close to CP El Niño years (Figs. 4a, e) were called intermediate CP El Niño conditions. Their spatial structure (Fig. 4e) is characterized by an anomaly core of about -0.04 mg m^{-3} located near 160°E. The persistent negative chlorophyll anomaly in the western Pacific could be specific to the period we study (recurring CP El Niño conditions) and this is why we do not refer to it as neutral conditions.

The SeaWiFS archive spans over more than 13 years during which 5 El Niño events occur. Interestingly, the AHC analysis we performed on the monthly surface chlorophyll anomaly maps separates the 1997-1998 EP episode from the other CP El Niño episodes. These results need to be refined with the help of longer observational time series, modeling outputs, and theoretical work. An improve understanding of the phytoplankton distribution and its temporal variability is actually essential to anticipate biogeochemical climate-driven shifts and their consequences on ocean dynamics, carbon cycle, and marine ressources. Different phytoplankton distribution during CP and EP El Niño events could actually impact the distribution and abundance of exploited fish species such as tuna, whose fishery in the central and western tropical Pacific is one of the largest industrial fisheries of the world [Lehodey et al., 2011]. Complementing our qualitative analysis, we also need to quantify how physical and/or biological processes lead to the contrasted patterns we evidenced.

Acknowledgements

We acknowledge the SeaWiFS Project at GSFC (http://oceancolor.gsfc.nasa.gov), the Hadley Centre for Climate Prediction and Research Sea Ice and Sea Surface Temperature (http://www.metoffice.gov.uk/hadobs/hadisst), OSCAR (http://www.oscar.noaa.gov), the SSS Observation Service (http://www.legos.obs-mip.fr/observations/sss), and the TOGA-TAO Project Office of NOAA/PMEL (http://www.pmel.noaa.gov/tao) for sharing the freely available data we used. We also used time series of the Southern Oscillation Index (http://www.cpc.ncep.noaa.gov/data/indices/soi) and of the El Niño Modoki Index (http://www.jamstec.go.jp/frcgc/research/d1/iod/modoki_home.html.en). This work was supported by CNES in the frame of the Ocean Surface Topography Science Team program. F. L. benefited from CNES funding and A. S. benefits from a PhD grant from the Institut de Recherche pour le Développement (IRD). We thank the two reviewers for their useful comments.

References

An, S.-I. and F.-F. Jin (2004), Nonlinearity and asymmetry of ENSO. *J. Clim., 17*, 2399–2412.

Ashok, K., S. K. Behera, S. A. Rao, H. Weng, and T .Yamagata (2007), El Niño Modoki and its teleconnection, *J. Geophys. Res., 112*, C11007, doi:10.1029/2006JC003798.

Barber, R. T. and J. E. Kogelschatz (1990), Nutrients and productivity during the 1982/83 El Niño. In: *Global ecological consequences of the 1982-83 El Niño-Southern oscillation*, edited by P. W. Glynn, pp. 31-53, Elsevier, Amsterdam.

Barber, R. T., M. P. Sanderson, S. T. Lindley, F. Chai, J. Newton, C. C. Trees, D. G. Foley, and F. P. Chavez (1996), Primary productivity and its regulation in the equatorial Pacific during and following the 1991-1992 El Niño. *Deep-Sea Res. II, 43*, 933-969.

Blanchot, J., M. Rodier, and A. Le Bouteiller (1992), Effect of El Niño Southern Oscillation events on the distribution and abundance of phytoplankton in the western Pacific Ocean along 165°E. *J. Plankton Res., 4*, 137-156.

Bonjean, F. and G.S.E. Lagerloef (2002), Diagnostic model and analysis of the surface currents in the tropical Pacific ocean. *J. Phys. Oceanogr., 32*, 2938-2954.

Bosc, C., T. Delcroix, and C. Maes (2009), Barrier layer variability in the western Pacific warm pool from 2000 to 2007, *J. Geophys. Res., 114*, C06023, doi:10.1029/2008JC005187.

Campbell, J. W., J. M. Blaisdell, and M. Darzi (1995), Level-3 SeaWiFS data products: Spatial and temporal binning algorithms, *NASA Technical Memorandum, 32*, 104566, 80 pp.

Chavez, F. P., K. R. Buck, K. H. Coale, J. H. Martin, G. R. DiTullio, N. A. Welschmeyer, A. C. Jacobson, and R. T. Barber (1991), Growth rates, grazing, sinking, and iron limitation of equatorial Pacific phytoplankton. *Limnol. Oceanogr., 36*, 1816-1833.

Chavez, F. P., P. G. Strutton, and M. J. McPhaden (1998), Biological-physical coupling in the central Pacific during the onset of the 1997-98 El Niño. *Geophys. Res. Lett., 25*, 3543-3546.

Chavez, F. P., P. G. Strutton, G. E. Friederich, R. A. Feely, G. C. Feeldman, D. G. Foley, and M. J. McPhaden (1999), Biological and chemical response of the equatorial Pacific Ocean to the 1997-98 El Niño. *Science, 286*, 2126-2131.

Christian, J. R., M. A. Verschell, R. Murtugudde, A. J. Busalacchi, and C. R. McClain (2002), Biogeochemical modelling of the tropical Pacific ocean. II. Iron biogeochemistry. *Deep-Sea Res. II, 49*, 545-565.

Christian, J. R., R. Murtugudde, J. Ballabrera-Poy, and C. R. McClain (2004), A ribbon of dark water: phytoplankton blooms in the meanders of the Pacific North Equatorial Countercurrent. *Deep-Sea Res. II, 51*, 209-228.

Delcroix, T., B. Dewitte, Y. duPenhoat, F. Masia, and J. Picaut (2000), Equatorial waves and warm pool displacements during the 1992-1998 El Niño Southern Oscillation events: Observation and modeling. *J. Geophys. Res., 105*, 14357-14373.

Delcroix, T., G. Alory, S. Cravatte, T. Corrège, and M. J. McPhaden (2011), A gridded sea surface salinity data set for the tropical Pacific with sample applications (1950–2008). *Deep-Sea Res. I, 58*, 38-48.

Eldin, G., M. Rodier, and M. H. Radenac (1997), Physical and nutrient variability in the upper equatorial Pacific associated with westerly wind forcing and wave activity in October 1994. *Deep-Sea Res. II, 44*, 1783-1800.

Evans, W., P. G. Strutton, and F. P. Chavez (2009), Impact of tropical instability waves on nutrient and chlorophyll distributions in the equatorial Pacific. *Deep-Sea Res. I, 56*, 178-188.

Friedrichs, M. A. M. and E. E. Hofmann (2001), Physical control of biological processes in the central equatorial Pacific Ocean. *Deep-Sea Res. I, 48*, 1023-1069.

Frouin, R., B. A. Franz and P. J. Werdell (2003), The SeaWiFS PAR product. In *Algorithm Updates for the Fourth SeaWiFS Data Reprocessing*, edited by S. B. Hooker and E. R. Firestone, pp. 46–50, NASA/TM-2003-206892, 22.

Glantz, M. H. (2000), *Currents of Change: Impacts of El Niño and La Niña on climate and society*. Cambridge, UK: Cambridge University Press. 266 pp.

Goes, J. I., K. Sasaoka, H. Do R. Gomes, S.-I. Saitoh, and T. Saino (2004), A comparison of the seasonality and interannual variability of phytoplankton biomass and production in the western and eastern gyres of the subarctic Pacific using multi-sensor satellite data. *J. Oceanogr., 60*, 75-91.

Gordon, R. M., K. H. Coale, and K. S. Johnson (1997), Iron distribution in the equatorial Pacific: Implications for new production. *Limnol. Oceanogr., 43*, 419-431.

Gorgues, T., C. Menkes, O. Aumont, J. Vialard, Y. Dandonneau, and L. Bopp (2005), Biogeochemical impact of tropical instability waves in the equatorial Pacific. *Geophys. Res. Lett., 32*, L24615, doi:10.1029/2005GL024110.

Gorgues, T., C. Menkes, L. Slemons, O. Aumont, Y. Dandonneau, M.-H. Radenac, S. Alvain, and C. Moulin (2010), Revisiting the La Niña 1998 phytoplankton blooms in the equatorial Pacific. *Deep-Sea Res. I, 57*, 567-576.

Hsieh W. W. (2001) Nonlinear canonical correlation analysis of the tropical Pacific climate variability using a neural network approach. *J. Clim., 14*, 2528–2539.

Izumo, T. (2005), The equatorial undercurrent, meridional overturning circulation, and their roles in mass and heat exchanges during El Niño events in the tropical Pacific ocean. *Ocean Dyn., 55*, 110-123.

Johnson, G. C., M. J. McPhaden, G. D. Rowe, and K. E. McTaggart (2000), Upper equatorial Pacific ocean current and salinity variability during the 1996-1998 El Niño-La Niña cycle. *J. Geophys. Res., 105*, 1037-1053.

Kao, H.-Y. and J.-Y. Yu (2009), Contrasting eastern-Pacific and central-Pacific types of ENSO. *J. Clim., 22*, 615-632.

Kim, H.-M., P. J. Webster, and J. A. Curry (2009), Impact of shifting patterns of Pacific ocean warming on north Atlantic tropical cyclones. *Science, 325*, 5936, 77-80.

Kim, W., S.-W. Yeh, J.-H. Kim, J.-S. Kug, and M. Kwon (2011), The unique 2009–2010 El Niño event: A fast phase transition of warm pool El Niño to La Niña, *Geophys. Res. Lett.*, 38, L15809, doi:10.1029/2011GL048521.

Kug, J.-S., and Y.-G. Ham (2011), Are there two types of La Nina?, *Geophys. Res. Lett., 38*, L16704, doi:10.1029/2011GL048237.

Kug, J.-S., F.-F. Jin, and S.-I. An (2009), Two types of El Niño events: cold tongue El Niño and warm pool El Niño. *J. Clim., 22*, 1499–1515, doi: 10.1175/2008JCLI2624.1.

Kuroda, Y. (2000), Variability of currents off the northern coast of New Guinea. *J. Oceanogr., 56*, 103-116.

Lacan, F. and C. Jeandel (2001), Tracing Papua New Guinea imprint on the central Equatorial Pacific Ocean using neodymium isotopic compositions and Rare Earth Element patterns. *Earth Planet. Sci. Lett., 186*, 497-512.

Landry, M. R., R. T. Barber, R. R. Bidigare, F. Chai, K. H. Coale, H. G. Dam, M. R. Lewis, S. T. Lindley, J. J. McCarthy, M. R. Roman, D. K. Stoecker, P. G. Verity, and J. R. White (1997), Iron and grazing constraints on primary production in the central equatorial Pacific: An EqPac synthesis. *Limnol. Oceanogr., 42*, 405-418.

Larkin, N. K. and D. E. Harrison (2002), ENSO warm (El Niño) and cold (La Niña) event life cycles: ocean surface anomaly patterns, their symmetries, asymmetries, and implications. *J. Clim., 15*, 1118-1140.

Le Borgne, R., R. T. Barber, T. Delcroix, H. Y. Inoue, D. J. Mackey, and M. Rodier (2002), Pacific warm pool and divergence: temporal and zonal variations on the equator and their effects on the biological pump. *Deep-Sea Res. II, 49*, 2471-2512.

Le Bouteiller, A. and J. Blanchot (1991), Size distribution and abundance of phytoplankton in the Pacific equatorial upwelling, *La Mer, 29*, 175-179.

Lee, T. and M. J. McPhaden (2010), Increasing intensity of El Niño in the central-equatorial Pacific, *Geophys. Res. Lett., 37*, L14603, doi:10.1029/2010GL044007.

Legeckis, R. (1977), Long waves in the eastern equatorial Pacific Ocean: A view from a geostationary satellite. *Science, 197*, 1179-1181.

Lehodey, P., J. Hampton, R. W. Brill, S. Nicol, I. Senina, B. Calmettes, H. O. Pörtner, L. Bopp, T. Ilyina, J. D. Bell, and J. Sibert (2011), Vulnerability of oceanic fisheries in the tropical Pacific to climate change. In: *Vulnerability of Tropical Pacific Fisheries and Aquaculture to Climate Change*. Edited by J. D. Bell, J. E. Johnson and A. J. Hobday, pp. 433-492, Secretariat of the Pacific Community, Noumea, New Caledonia.

Leloup, J., M. Lengaigne, and J.-P. Boulanger (2007), Twentieth century ENSO characteristics in the IPCC database. *Clim. Dyn., 30*, 277-291.

Letelier, R. M., D. M. Karl, M. R. Abbott and R. R. Bidigare (2004), Light driven seasonal patterns of chlorophyll and nitrate in the lower euphotic zone of the north pacific subtropical gyre. *Limnol. Oceanogr., 49*, 508-519.

Mackey, D. J., J. Parslow, H. W. Higgins, F. B. Griffiths, and J. E. O'Sullivan (1995), Plankton productivity and biomass in the western equatorial Pacific: biological and physical controls. *Deep-Sea Res. II, 42*, 499-533.

Maes, C., J. Picaut, Y. Kuroda, and K. Ando (2004), Characteristics of the convergence zone at the eastern edge of the Pacific warm pool. *Geophys. Res. Lett., 31*, L11304, doi: 10.1029/2004GL019867.

McClain, C. R., G. C. Feldman, and S. B. Hooker (2004), An overview of the SeaWiFS project and strategies for producing a climate research quality global ocean bio-optical time series. *Deep-Sea Res. II, 51*, 5-42.

McPhaden, M. J., A. J. Busalacchi, R. Cheney, J.-R. Donguy, K. S. Gage, D. Halpern, M. Ji, P. Julian, G. Meyers, G. T. Mitchum, P. P. Niiler, J. Picaut, R. W. Reynolds, N. Smith, and K. Takeuchi (1998), The Tropical Ocean-Global Atmosphere observing system: A decade of progress. *J. Geophys. Res., 103*, 14169-14240.

McPhaden, M. J., S. E. Zebiak, and M. H. Glantz (2006), ENSO as an integrating concept in Earth science, *Science, 314*, 5806, 1740-1745, doi:10.1126/science.1132588.

McPhaden, M. J., T. Lee, and D. McClurg (2011), El Niño and its relationship to changing background conditions in the tropical Pacific Ocean, *Geophys. Res. Lett., 38*, L15709, doi:10.1029/2011GL048275.

Menkes, C., S. C. Kennan, P. Flament, Y. Dandonneau, S. Masson, B. Biessy, E. Marchal, G. Eldin, J. Grelet, Y. Montel, A. Morliere, A. Lebourges-Dhaussy, C. Moulin, G. Champalbert and, A. Herbland (2002), A whirling ecosystem in the Equatorial Atlantic, *Geophys. Res. Lett., 11*, 1553, doi: 10.1029/2001GL014576.

Messié, M. (2006), Contrôle de la dynamique de la biomasse phytoplanctonique dans le Pacifique tropical ouest. Thèse de doctorat de l'Univ. Toulouse 3, France, 263 pp.

Messié, M. and M.-H. Radenac (2006), Seasonal variability of the surface chlorophyll in the western tropical Pacific from SeaWiFS data. *Deep-Sea Res. I, 53*, 10, 1581-1600.

Messié, M., M.-H. Radenac, J. Lefèvre, and P. Marchesiello (2006), Chlorophyll bloom in the western Pacific at the end of the 1997-98 El Niño: the role of Kiribati Islands, *Geophys. Res. Lett., 33*, L14601, doi:10.1029/2006GL026033.

Murtuggude, R. G., S. R. Signorini, J. R. Christian, A. J. Busalacchi, C. R. McClain, and J. Picaut (1999), Ocean color variability of the tropical Indo-Pacific basin observed by SeaWiFS during 1997-98. *J. Geophys. Res., 104*, 18351-18365.

Park, J.-Y., J.-S. Kug, J.-S. Park, S.-W. Yeh, and C. J. Jang (2011), Variability of chlorophyll associated with ENSO and its possible biological feedback in the Equatorial Pacific, *J. Geophys. Res.*, doi:10.1029/2011JC007056.

Picaut, J. and T. Delcroix (1995), Equatorial wave sequence associated with warm pool displacement during the 1986-1989 El Niño-La Niña. *J. Geophys. Res., 100*, 18393-18408.

Picaut, J., M. Ioualalen, T. Delcroix, F. Masia, R. Murtugudde, and J. Vialard (2001), The oceanic zone of convergence on the eastern edge of the Pacific warm pool: A synthesis of results and implications for El Niño-Southern Oscillation and biogeochemical phenomena. *J. Geophys. Res., 106*, 2363-2386.

Poulain, P.-M. (1993), Estimates of horizontal divergence and vertical velocity in the equatorial Pacific. *J. Phys. Oceanogr., 23*, 601-607.

Radenac, M.-H. and M. Rodier (1996), Nitrate and chlorophyll distributions in relation to thermohaline and current structures in the western tropical Pacific during 1985-1989. *Deep-Sea Res. II, 43*, 725-752.

Radenac, M.-H., C. Menkes, J. Vialard, C. Moulin, Y. Dandonneau, T. Delcroix, C. Dupouy, A. Stoens, and P.-Y. Deschamps (2001), Modeled and observed impacts of the 1997-1998 El Niño on nitrate and new production in the equatorial Pacific, *J. Geophys. Res., 106*, 26879-26898.

Radenac, M.-H., Y. Dandonneau, and B. Blanke (2005), Displacements and transformations of nitrate-rich and nitrate-poor water masses in the tropical Pacific during the 1997 El Niño, *Ocean Dyn., 55*, 34-46, DOI: 10.1007/s10236-005-0111-5.

Radenac, M.-H., P. E. Plimpton, A. Lebourges-Dhaussy, L. Commien, and M. J. McPhaden (2010), Impact of environmental forcing on the acoustic backscattering strength in the equatorial Pacific: diurnal, lunar, intraseasonal, and interannual variability, *Deep-Sea Res. I, 57*, 1314-1328.

Rasmusson, E. M. and T. H. Carpenter (1982), Variations in tropical sea surface temperature and surface wind fields associated with the Southern Oscillation/El Niño. *Mon. Weather Rev., 110*, 354–384.

Rayner, N. A., D. E. Parker, E. B. Horton, C. K. Folland, L. V. Alexander, D. P. Rowell, E. C. Kent, and A. Kaplan (2003), Global analyses of sea surface temperature, sea ice, and night marine air temperature since the late nineteenth century, *J. Geophys. Res., 108*, 4407, doi:10.1029/2002JD002670.

Rébert, J.-P., J.-R. Donguy, G. Eldin, and K. Wyrtki (1985), Relations between sea-level, thermocline depth, heat content, and dynamic height in the tropical Pacific. *J. Geophys. Res., 90*, 11719-11725.

Ren, H.-L. and F.-F. Jin (2011), Niño indices for two types of ENSO, *Geophys. Res. Lett., 38*, L04704, doi:10.1029/2010GL046031.

Ryan, J. P., P. S. Polito, P. G. Strutton, and F. P. Chavez (2002), Unusual large-scale phytoplankton blooms in the equatorial Pacific. *Prog. Oceanogr., 55*, 263-285.

Ryan, J. P., I. Ueki, Y. Chao, H. Zhang, P. S. Polito, and F. P. Chavez (2006), Western Pacific modulation of large phytoplankton blooms in the central and eastern equatorial Pacific. *J. Geophys. Res., 111*, G02013, doi: 10.1029/2005JG000084.

Singh, A., T. Delcroix, and S. Cravatte (2011), Contrasting the flavors of El Niño-Southern Oscillation using sea surface salinity observations. *J. Geophys. Res., 116*, C06016, doi:10.1029/2010JC006862.

Singh, A., and T. Delcroix (2011), Estimating the effects of ENSO upon the observed freshening trends of the western tropical Pacific Ocean. *Geophys. Res. Lett., 38*, L21607, doi:10.1029/2011GL049636.

Slemons, L. O., J. W. Murray, J. Resing, B. Paul, and P. Dutrieux (2010), Western Pacific coastal sources of iron, manganese, and aluminum to the Equatorial Undercurrent, *Global Biogeochem. Cycles, 24*, GB3024, doi:10.1029/2009GB003693.

Stoens, A., C. Menkes, M.-H. Radenac, N. Grima, Y. Dandonneau, G. Eldin, L. Memery, C. Navarette, J.-M. André, T. Moutin, and P. Raimbault (1999), The coupled physical-new production system in the equatorial Pacific during the 1992-1995 El Niño. *J. Geophys. Res., 104*, 3323-3339.

Strutton, P. G. and F. P. Chavez (2000), Primary productivity in the equatorial Pacific during the 1997-98 El Niño. *J. Geophys. Res., 105*, 26089-26101.

Strutton, P. G., J. P.Ryan, and F. P.Chavez (2001), Enhanced chlorophyll associated with tropical instability waves in the equatorial Pacific. *Geophys. Res. Lett., 28*, 2005-2008.

Strutton, P. G., W. Evans, and F. P. Chavez (2008), Equatorial Pacific chemical and biological variability, 1997-2003. *Global Biogeochem. Cycles,* 22, GB2001, doi:10.1029/2007GB003045.

Takahashi, K., A. Montecinos, K. Goubanova, and B. Dewitte (2011), ENSO regimes: Reinterpreting the canonical and Modoki El Niño, *Geophys. Res. Lett., 38*, L10704, doi:10.1029/2011GL047364.

Trenberth, K. E. and D. P. Stepaniak (2001), Indices of El Niño evolution. *J. Clim., 14*, 1697-1701.

Turk, D., M. R. Lewis, G. W. Harrison, T. Kawano, and I. Asanuma (2001), Geographical distribution of new production in the western/central equatorial Pacific during El Niño and non-El Niño conditions. *J. Geophys. Res., 106*, 4501-4515.

Turk, D., C. S. Meinen, D. Antoine, M. J. McPhaden, and M. R. Lewis (2011), Implications of changing El Niño patterns for biological dynamics in the equatorial Pacific Ocean. *Geophys. Res. Lett.*, doi:10.1029/2011GL049674, in press.

Ueki, I., Y. Kashino, and Y. Kuroda (2003), Observation of current variations off the New Guinea coast including the 1997-1998 El Niño period and their relationship with Sverdrup transport. *J. Geophys. Res., 108*, 3243, doi:10.1029/2002JC001611.

Vialard, J., C. Menkes, J.-P. Boulanger, P. Delecluse, E. Guilyardi, M. J. McPhaden, and G. Madec (2001), A model study of oceanic mechanisms affecting equatorial Pacific sea surface temperature during the 1997-98 El Niño. J.*Phys. Oceanogr., 31*, 1649-1675.

Vichi, M., S. Masina, and F. Nencioli (2008), A process-oriented model study of equatorial Pacific phytoplankton: The role of iron supply and tropical instability waves. *Prog. Oceanogr., 78*, 147-162.

Vincent, E. M., M. Lengaigne, C. E. Menkes, N. C. Jourdain, P. Marchesiello and G. Madec (2009), Interannual variability of the South Pacific Convergence Zone and implications for tropical cyclone genesis. *Clim. Dyn*., DOI 10.1007/s00382-009-0716-3.

Webster, P. J. and R. Lukas (1992), TOGA-COARE: the Coupled Ocean-Atmosphere Response Experiment. *Bull. Am. Meteorol. Soc., 73*, 1377-1416.

Wells, M. L., G. K. Vallis, and E. A. Silver (1999), Tectonic processes in Papua New Guinea and past productivity in the eastern equatorial Pacific Ocean. *Nature, 398*, 6728, 601-604.

Wilson, C. and D. Adamec (2001), Correlations between surface chlorophyll and sea surface height in the tropical Pacific during the 1997-1999 El Niño-Southern Oscillation event. *J. Geophys. Res., 106*, 31175-31188.

Yeh, S.-W., J.-S. Kug, B. Dewitte, M.-H. Kwon, B. P. Kirtman, and F.-F. Jin (2009), El Niño in a changing climate. *Nature, 416*, 511-514.

Yoder, J. A. and M. Kennelly (2003), Seasonal and ENSO variability in global ocean phytoplankton chlorophyll derived from 4 years of SeaWiFS measurements. *Global Biogeochem. Cycles, 17*, 1112, doi: 10.1029/2002GB001942.

Yoder, J. A., S. G. Ackleson, R. T. Barber, P. Flament and W. M. Balch (1994), A line in the sea. *Nature, 371*, 689– 692.

Yu, J.-Y. and S. T. Kim (2010), Identification of Central-Pacific and Eastern-Pacific types of ENSO in CMIP3 models, *Geophys. Res. Lett., 37*, L15705, doi:10.1029/2010GL044082.

Yu, J.-Y., H.-Y. Kao, T. Lee, and S. T. Kim (2010), Subsurface ocean temperature indices for central-Pacific and eastern-Pacific types of El Nino and La Nina events. *Theor. Appl. Climatol.*, DOI: 10.1007/s00704-010-0307-6.

Table 1. Classification of ENSO events as Central Pacific (CP) or Eastern Pacific (EP) El Niño (EN) or La Niña (LN). All studies used SST except (1) used SSS and (2) used chlorophyll to characterize ENSO.

	97-98	98-99	99-00	00-01	02-03	04-05	05-06	06-07	07-08	08-09	09-10	10
Ashok et al. [2007]					CP EN	CP EN						
Kim et al. [2009]	EP EN	EP LN	EP LN		CP EN	CP EN						
Yeh et al. [2009]	EP EN				CP EN	CP EN		EP EN				
Kao and Yu [2009]	EP EN	CP LN	CP LN		CP EN	CP EN	EP LN					
Kug et al. [2009]	EP EN	LN	LN	LN	CP EN	CP EN	LN					
Lee and McPhaden [2010]	EP EN	LN			CP EN	CP EN		EP EN	LN		CP EN	
Ren and Jin [2011]	EP EN	LN	LN		CP EN	CP EN		CP EN	LN		CP EN	
(1)Singh et al. [2011]	EP EN	CP LN	EP LN	EP LN	CP EN	CP EN	EP LN	CP EN	EP LN	EP LN		
McPhaden et al. [2011]	EP EN				CP EN	CP EN		EP EN			CP EN	
(2)This study	EP EN	LN	LN	LN	CP EN	CP EN		CP EN	LN	LN	CP EN	LN

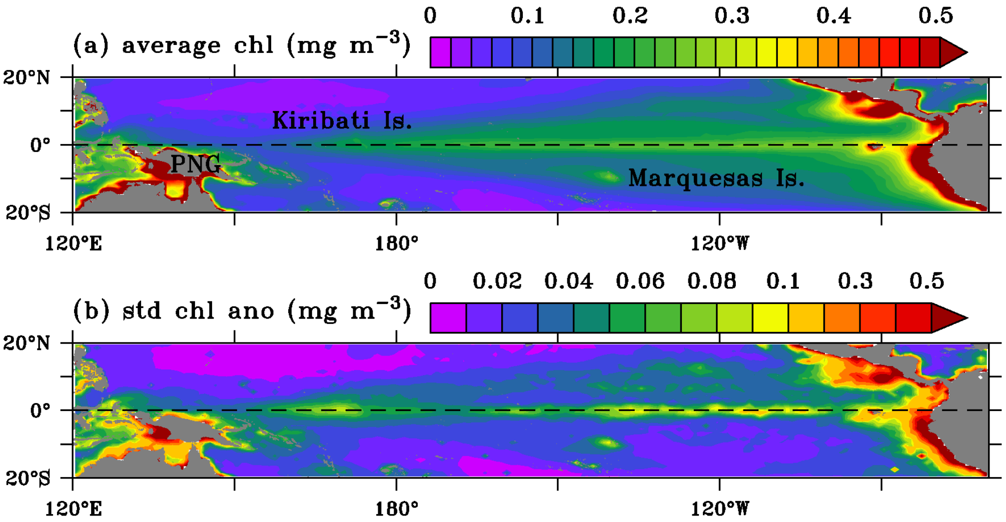

Figure 1. Maps of (a) average and (b) interannual standard deviation of the surface chlorophyll computed over the September 1997 - December 2010 period. PNG stands for Papua New Guinea.

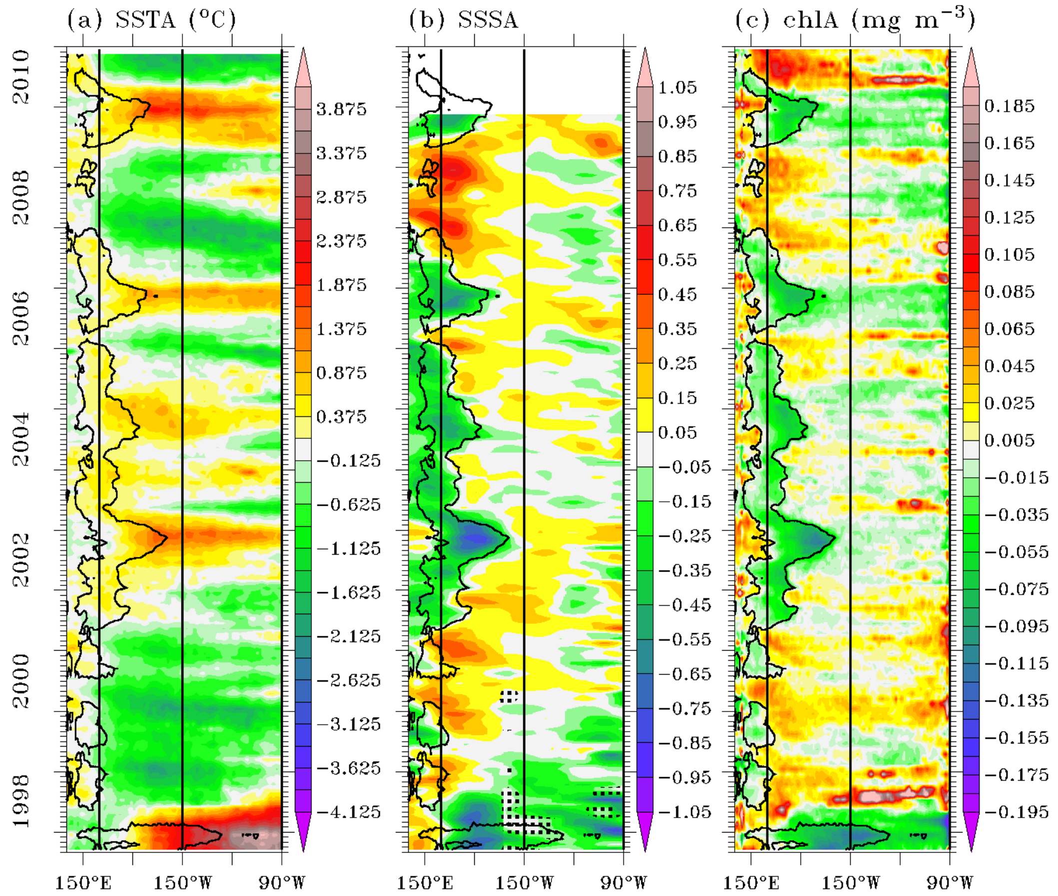

Figure 2. Longitude-time distribution of the anomaly of (a) SST, (b) SSS, and (c) surface chlorophyll averaged between 5°S and 5°N. The black contour encloses the region with surface chlorophyll lower than 0.1 mg m^{-3}. Vertical lines indicate the zonal boundaries of the Niño3 (150°W, 90°W) and Niño4 (160°E, 150°W) regions. Regions with dots in (b) indicate normalized SSS errors larger than 0.80.

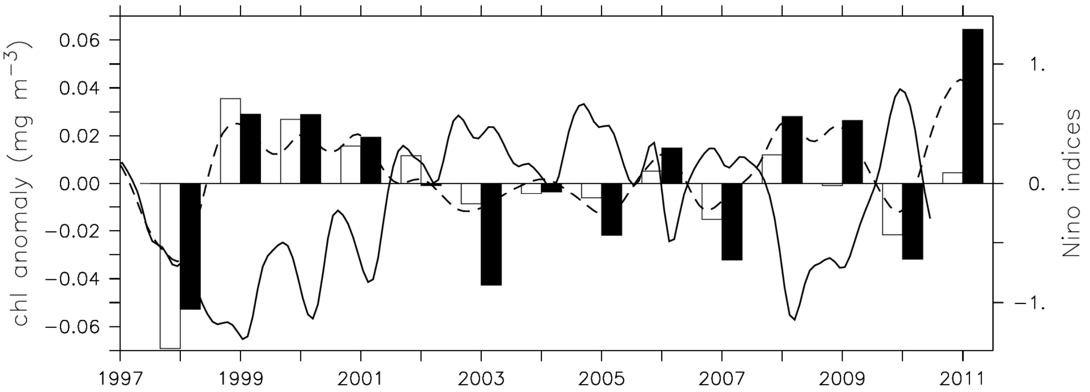

Figure 3. Surface chlorophyll anomaly averaged between September and February in the Niño3 (150°W-90°W, 5°S-5°N; hollow bars) and Niño4 (160°E-150°W, 5°S-5°N; filled bars) regions. EMI (full line) and 0.25×SOI (dashed line) are scaled on the right axis.

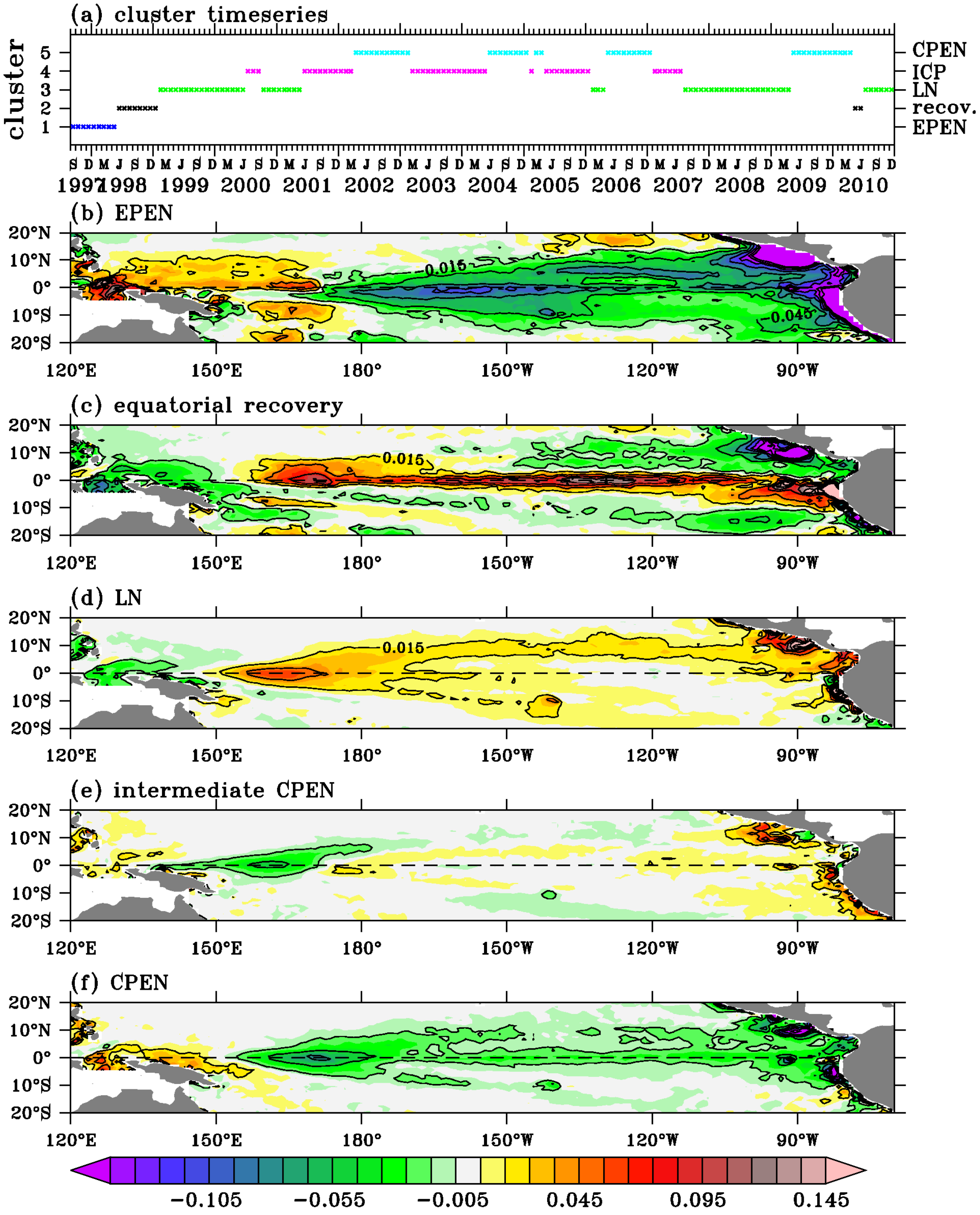

Figure 4. (a) Time series of the cluster analysis. Spatial patterns of the corresponding surface chlorophyll anomaly during the so-called (b) Eastern Pacific El Niño (EPEN), (c) equatorial recovery conditions (recov), (d) La Niña (LN), (e) intermediate Central Pacific period (ICP), and (f) Central Pacific El Niño (CPEN). Chlorophyll anomaly contours are every 0.03 mg m^{-3}. The 0 mg m^{-3} contour is omitted.

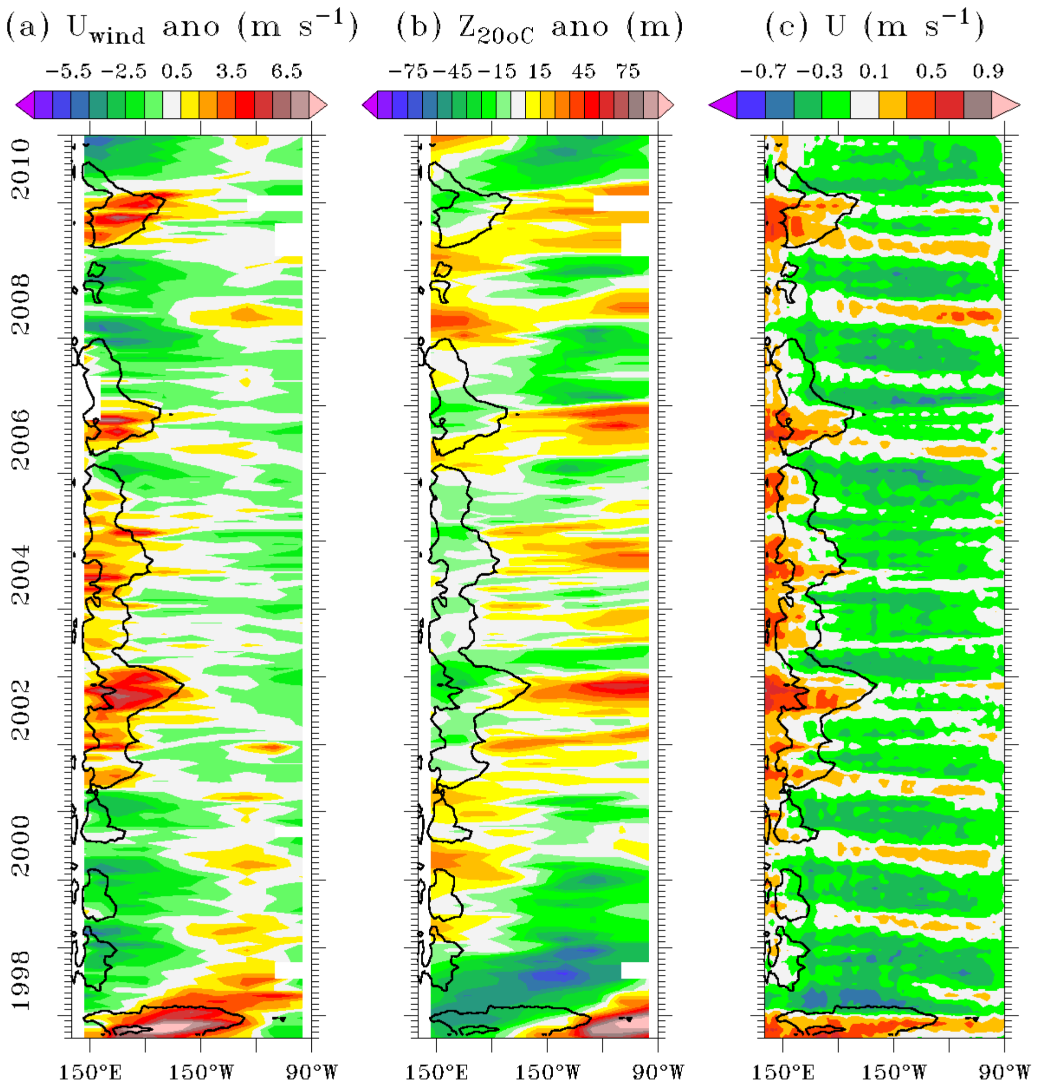

Figure 5. Longitude-time distribution along the equator of (a) zonal wind speed anomaly (positive eastwards; colors; m s^{-1}), (b) 20°C isotherm depth anomaly (positive downward; m), and (c) zonal surface current (positive eastwards; m s^{-1}). The black contours in (a-c) enclose the region with surface chlorophyll lower than 0.1 mg m^{-3}.

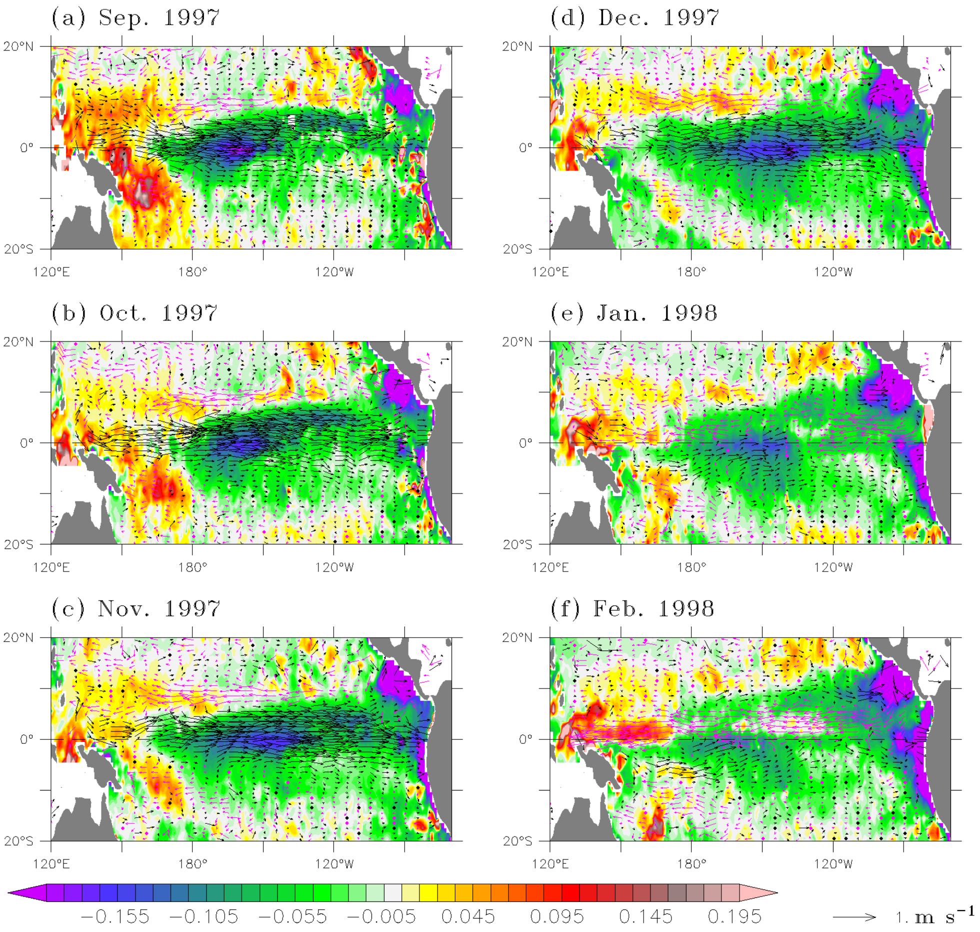

Figure 6. Maps of monthly surface chlorophyll anomaly (colors; mg m^{-3}) and surface layer current anomaly (vectors; m s^{-1}) during the 1997-1998 Eastern Pacific El Niño. Current vectors with eastward (westward) zonal component are in black (purple).

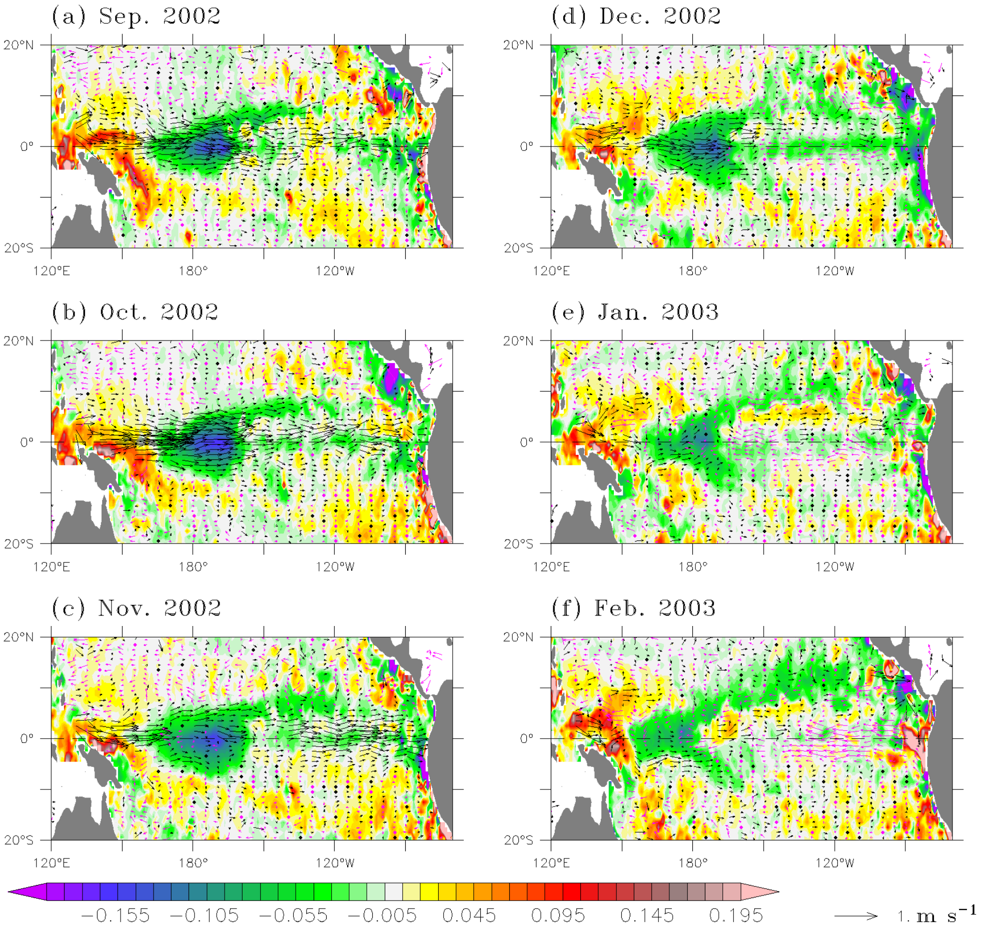

Figure 7. Maps of monthly surface chlorophyll anomaly (colors; mg m^{-3}) and surface layer current anomaly (vectors; m s^{-1}) during the 2002-2003 Central Pacific El Niño. Current vectors with eastward (westward) zonal component are in black (purple).

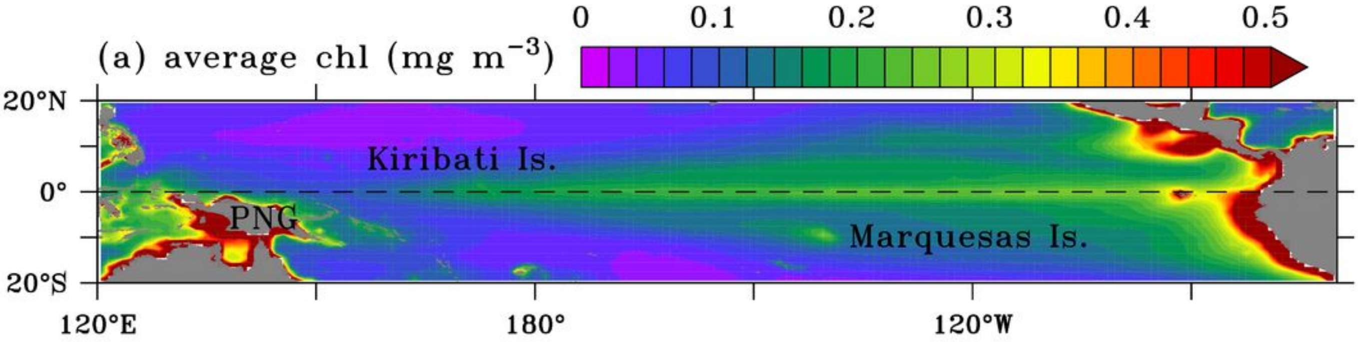

(a) average chl (mg m^{-3})

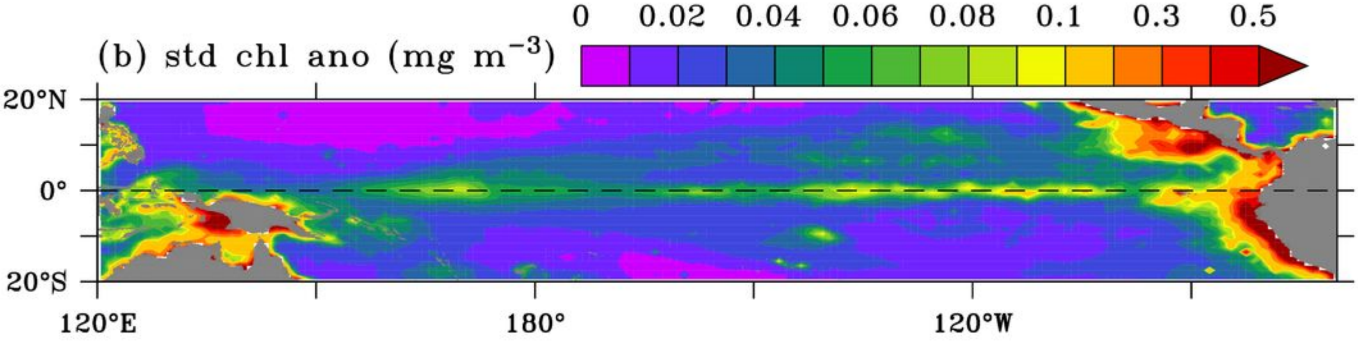

(b) std chl ano (mg m^{-3})

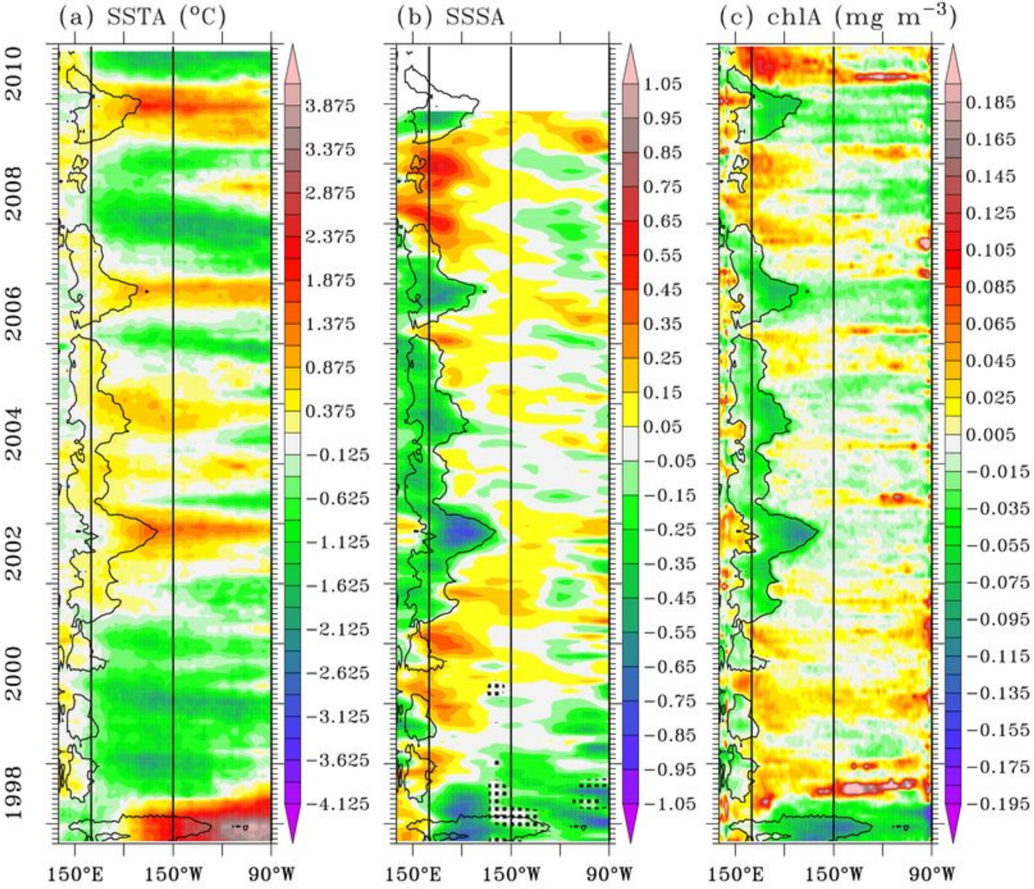
(a) SSTA (°C)
(b) SSSA
(c) chlA (mg m^{-3})
2010
2008
2006
2004
2002
2000
1998
150°E
150°W
90°W
3.875
3.375
2.875
2.375
1.875
1.375
0.875
0.375
−0.125
−0.625
−1.125
−1.625
−2.125
−2.625
−3.125
−3.625
−4.125
1.05
0.95
0.85
0.75
0.65
0.55
0.45
0.35
0.25
0.15
0.05
−0.05
−0.15
−0.25
−0.35
−0.45
−0.55
−0.65
−0.75
−0.85
−0.95
−1.05
0.185
0.165
0.145
0.125
0.105
0.085
0.065
0.045
0.025
0.005
−0.015
−0.035
−0.055
−0.075
−0.095
−0.115
−0.135
−0.155
−0.175
−0.195

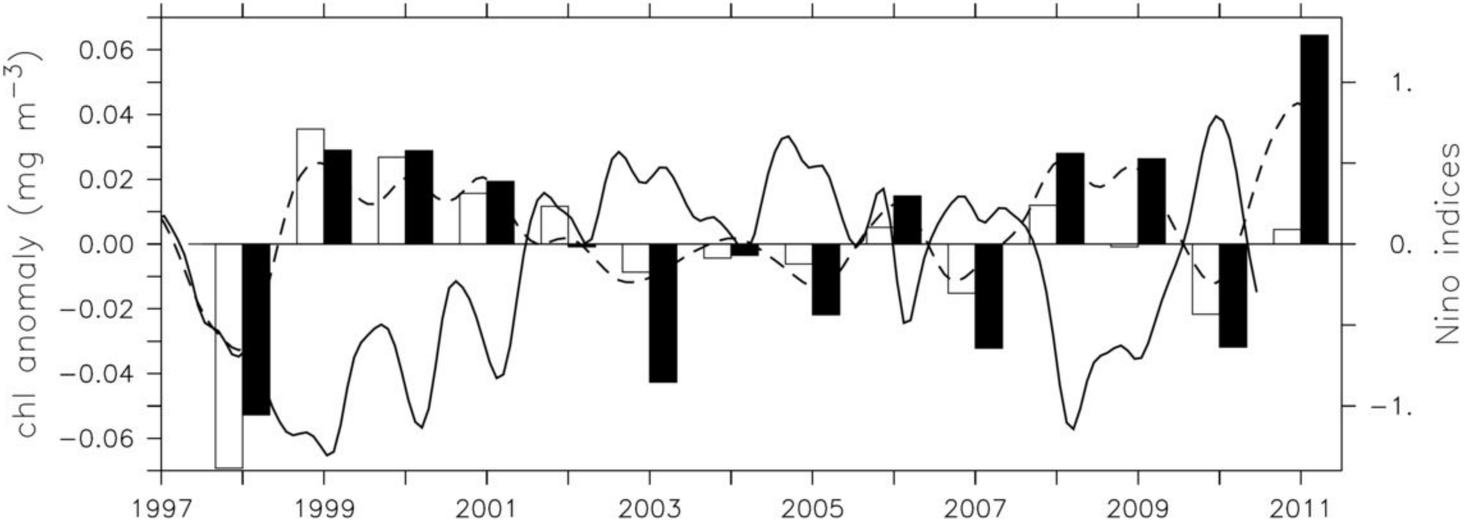
chl anomaly (mg m^{-3})
0.06
0.04
0.02
0.00
−0.02
−0.04
−0.06
Nino indices
1.
0.
−1.
1997
1999
2001
2003
2005
2007
2009
2011

(a) cluster timeseries

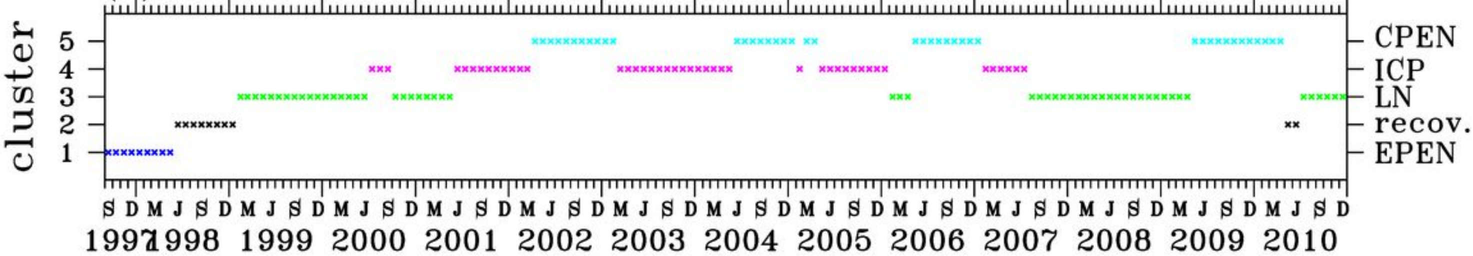

(b) EPEN

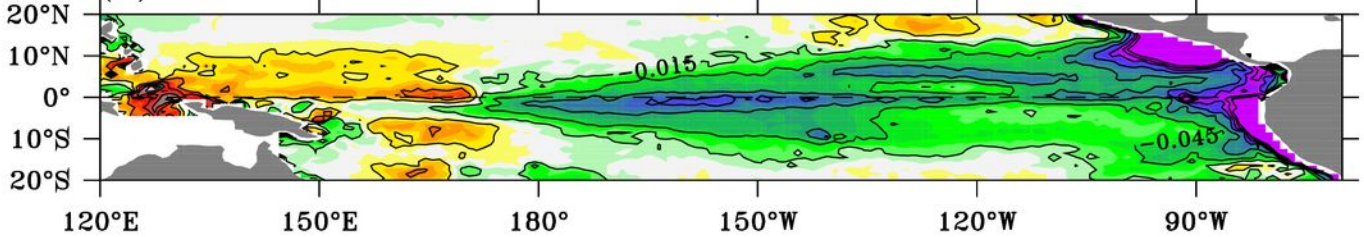

(c) equatorial recovery

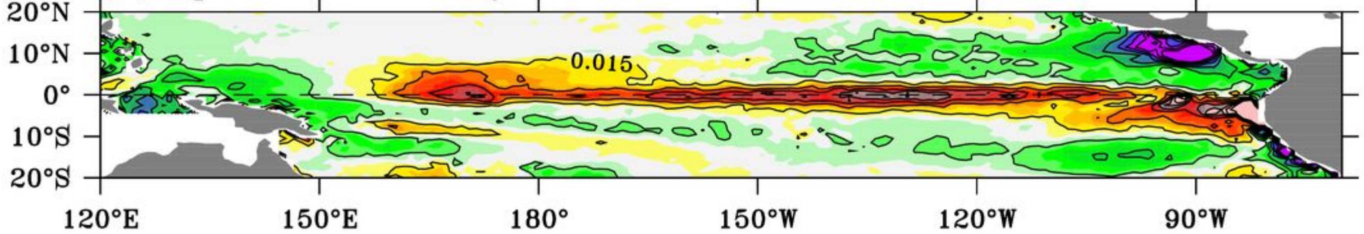

(d) LN

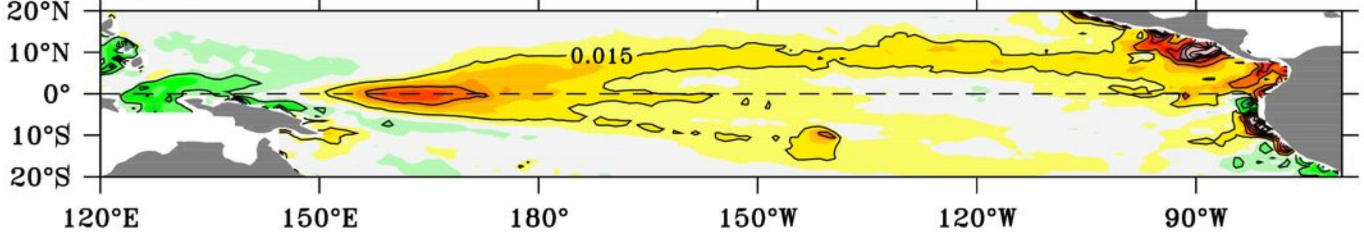

(e) intermediate CPEN

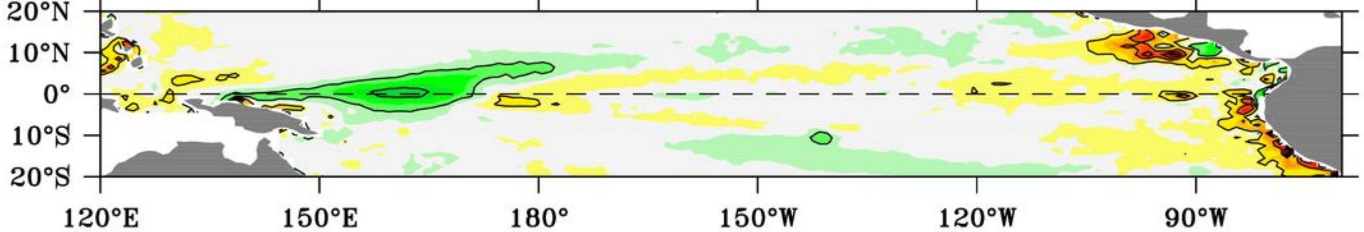

(f) CPEN

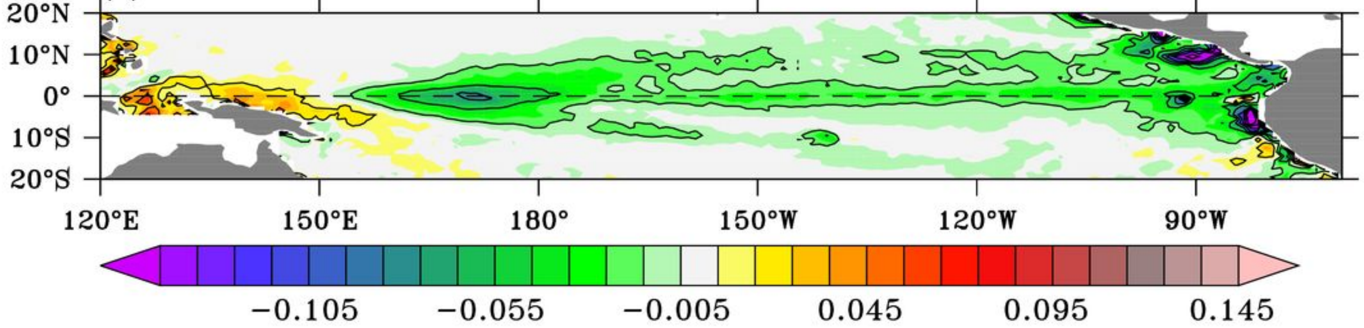

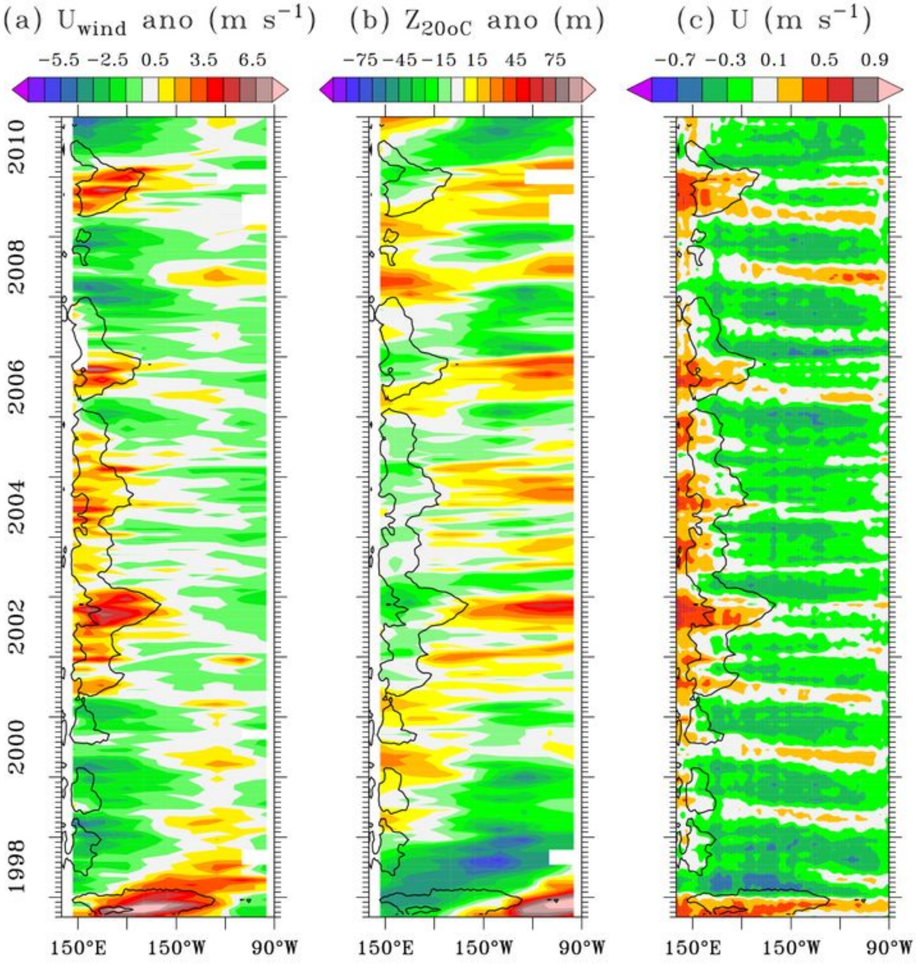
(a) U_{wind} ano ($m\ s^{-1}$)
−5.5 −2.5 0.5 3.5 6.5
(b) Z_{20oC} ano (m)
−75 −45 −15 15 45 75
(c) U ($m\ s^{-1}$)
−0.7 −0.3 0.1 0.5 0.9
2010
2008
2006
2004
2002
2000
1998
150°E
150°W
90°W

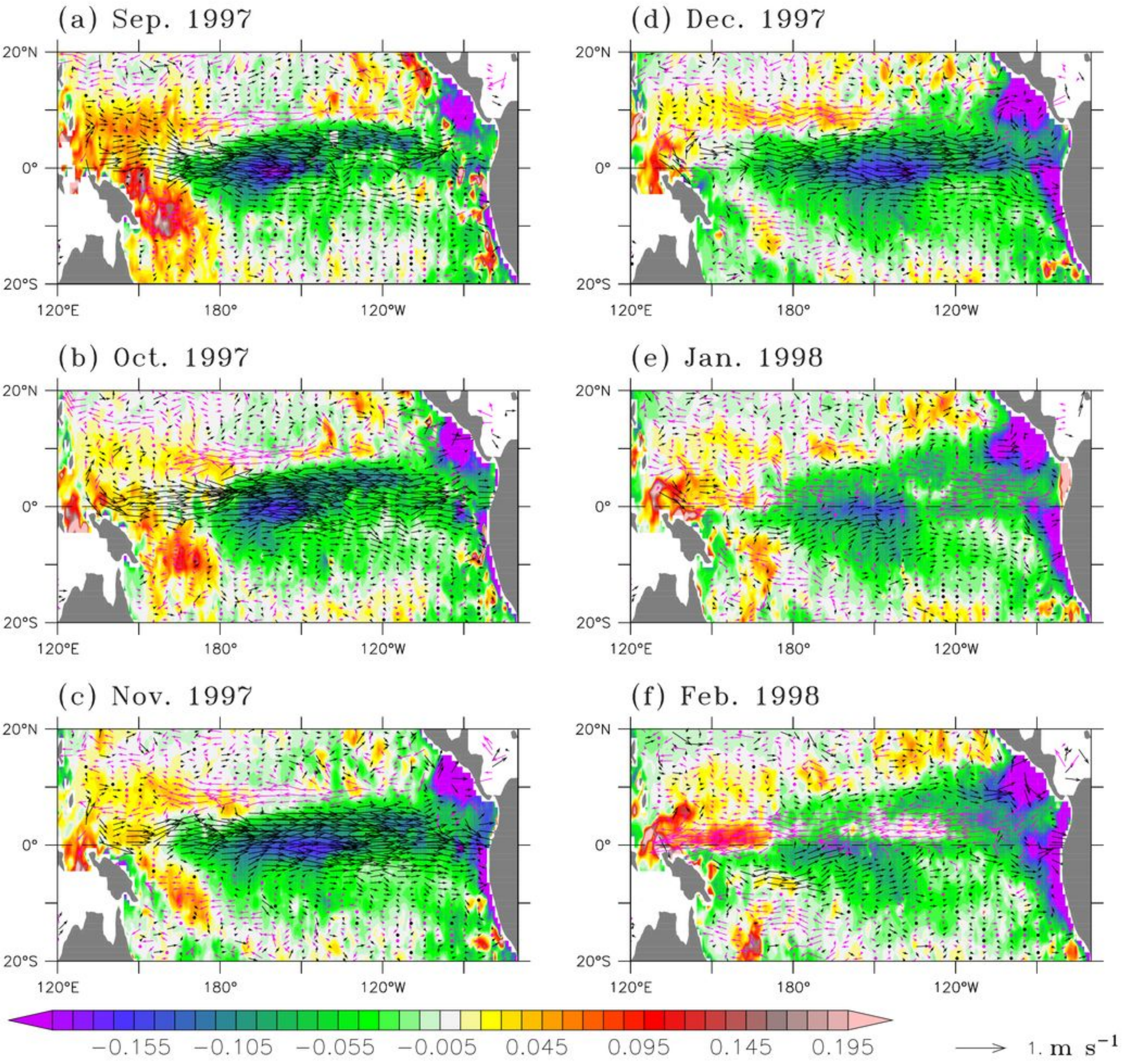
(a) Sep. 1997
(b) Oct. 1997
(c) Nov. 1997
(d) Dec. 1997
(e) Jan. 1998
(f) Feb. 1998
20°N
0°
20°S
120°E
180°
120°W
−0.155
−0.105
−0.055
−0.005
0.045
0.095
0.145
0.195
1. m s^{-1}

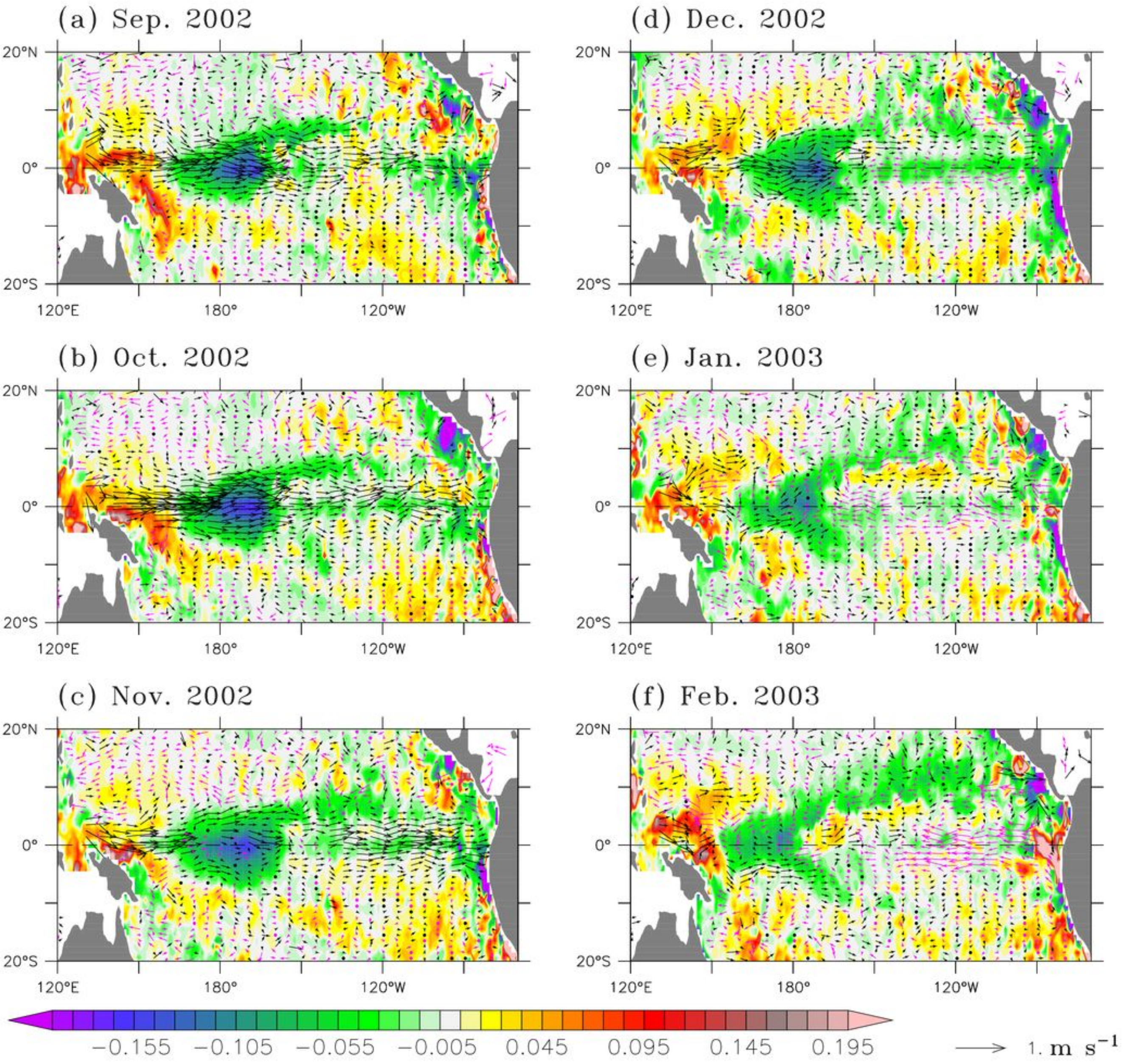
(a) Sep. 2002

(b) Oct. 2002

(c) Nov. 2002

(d) Dec. 2002

(e) Jan. 2003

(f) Feb. 2003